

# **LOW COHERENCE INTERFEROMETER FOR METROLOGY OF LIQUID-JET POLISHING OF LIGO OPTICS**

**M. Tech. Thesis**

*By*

**NAVEEN KUMAR**



**DISCIPLINE OF MECHANICAL ENGINEERING  
INDIAN INSTITUTE OF TECHNOLOGY INDORE**

**MAY 2025**

# **LOW COHERENCE INTERFEROMETER FOR METROLOGY OF LIQUID-JET POLISHING OF LIGO OPTICS**

**A THESIS**

*submitted in partial fulfillment of the  
requirements for the award of the degree*

*of*

**Master of Technology**

*by*

**NAVEEN KUMAR**



**DISCIPLINE OF MECHANICAL ENGINEERING  
INDIAN INSTITUTE OF TECHNOLOGY INDORE**

**MAY 2025**

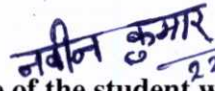


# INDIAN INSTITUTE OF TECHNOLOGY INDORE

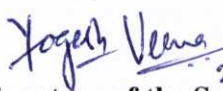
## CANDIDATE'S DECLARATION

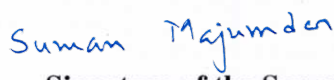
I hereby certify that the work which is being presented in the thesis entitled **LOW COHERENCE INTERFEROMETER FOR METROLOGY OF LIQUID-JET POLISHING OF LIGO OPTICS**, in partial fulfillment of the requirements for the award of the degree of **MASTER OF TECHNOLOGY** and submitted in the **DISCIPLINE OF MECHANICAL ENGINEERING**, Indian Institute of Technology Indore, is an authentic record of my own work carried out during the time period from **June 2024** to **May 2025**, under the supervision of **Dr. Yogesh Verma, SO/G (ALOD-RRCAT)** and **Shri Brijesh Chandra Pant, SO/F (ALOD-RRCAT)** and **Dr. Suman Majumdar, Associate Professor, DAASE IIT, Indore**.

The matter presented in this thesis has not been submitted by me for the award of any other degree of this or any other institute.

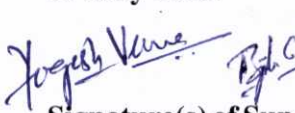
  
Signature of the student with date  
(NAVEEN KUMAR)


-----  
This is to certify that the above statement made by the candidate is correct to the best of my/our knowledge.

  
Signature of the Supervisor of  
M. Tech. thesis #1 (with date)  
(Dr. Yogesh Verma)

  
Signature of the Supervisor of  
M. Tech. thesis #2 (with date)  
(Dr. Suman Majumdar)

-----  
NAVEEN KUMAR has successfully given his M.Tech. Oral Examination held on 09 May 2025.

  
Signature(s) of Supervisor(s) of M.Tech. Thesis  
Date: 22-5-25

  
Convener, DPGC  
Date: 23-05-25

Signature of PSPC Member #1  
Date:

Signature of PSPC Member #2  
Date:

## ACKNOWLEDGEMENTS

I would like to sincerely thank my guide Dr. Yogesh Verma from Advanced Lasers and Optics Division (ALOD), RRCAT for his continuous support, guidance, and encouragement during my M.Tech project. His help and ideas were very important for completing this work.

I want to express my gratitude to Mr. Brijesh Chandra Pant from ALOD, RRCAT for helping me in the opto-mechanical design and development. His experience was very helpful in building the system.

I am also very thankful to Dr. Suman Majumdar from IIT Indore for his valuable support and advice in my project.

A big thanks to Dr. Sendhil Raja S., Head of the ALOD at RRCAT, for giving me the opportunity to work in this lab and for his kind support throughout the project.

I am thankful to the Opto-mechanical technical staff in the lab for helping with the design and assembly of the mechanical parts.

I would also like to thank Mr. Sharad for his help with the electronics, which was an important part of my work.

A very special thanks to Mr. Subhamoy Chakraborty for being a great support in my project for always being there with help, guidance, and encouragement. His time to time support from alignment of the optical setup to processing of the data was important for completion of project as well as over all understanding of the subject.

Finally, I thank all my friends, lab members, and my family for their constant support and motivation during my M. Tech journey.



# Abstract

Accurate surface measurement is very important when making high-quality optical components, such as those used in the LIGO experiment for detecting gravitational waves. Liquid Jet Polishing (LJP) is one of the promising techniques that can achieve high surface quality by removing the residual errors from the polished surface. For this, it uses pressurized liquid slurry of abrasive fluid for time dependent removal of material from the surface. To achieve precision optics it is utmost important to have a suitable measurement system that can provide the residual errors present in the optics accurately. In view of this a diffraction phase interferometer was developed that can provide nanometer scale the surface map across the sample surface. This thesis explains the development of a Low Coherence based Diffraction Phase Imaging (DPI) system to measure surface profile of the sample under test.

The DPI system was built using a Super luminescent Diode (SLD) as a low-coherence light source. It included a custom 4f imaging system and a pinhole to filter the light and capture clear phase information. Along with this, a prototype Liquid Jet Polishing (LJP) setup was also developed to generate the test samples that can be used to image using DPI system. Efforts were also made to assess the effect of important parameters such as nozzle size, slurry pressure, distance between nozzle and surface, and the movement speed of the sample stage.

Initially, We are presented the design and development of a prototype Liquid Jet Polishing (LJP) system for achieving ultra-polished optical surfaces. The prototype system, comprising a high-pressure pump, a 1 mm as well as 700  $\mu\text{m}$  diameter nozzle, and a precision sample holder, was tested for parameters such as stand-off distance (5 mm), pressure (8 bar), and exposure times of 60 sec and 90 sec. Initial experiments demonstrated material removal with dig diameters of 3 mm and 4 mm for exposure times of 60 and 90 seconds, respectively. The surface characteristics of the polished samples were evaluated using a transmission mode diffraction phase imaging interferometer, which resolves the material removal depths up to 1 micrometer from the phase maps.

Measurements were done on BK7 glass plates for different process parameters of the LJP system. The DPI system successfully measured small surface changes up to about 800 nanometers. Its results were confirmed by comparing them with a stylus-based surface measurement tool.

# Contents

<b>Abstract</b>	<b>iii</b>
<b>1 Interferometry</b>	<b>1</b>
1.1 Introduction . . . . .	1
1.1.1 Michelson Interferometer . . . . .	3
1.1.2 Fabry–Perot interferometer . . . . .	4
1.1.3 Coherence Interferometer . . . . .	5
1.1.4 Low Coherence Interferometer . . . . .	6
1.1.5 Application of low coherence interferometry . . . . .	7
<b>2 Diffraction Phase Imaging (DPI) Technique</b>	<b>8</b>
2.1 Introduction . . . . .	8
2.1.1 Transmission mode Diffraction Phase Imaging . . . . .	9
2.1.2 Reflection mode Diffraction Phase Imaging . . . . .	10
2.2 Development of prototype transmission mode DPI system . . . . .	11
2.2.1 Light Source and Collimation . . . . .	13
2.2.2 Sample Illumination and first 4f Imaging System . . . . .	13
2.2.3 Diffraction Grating . . . . .	14
2.2.4 Second 4f imaging system and masking using pinhole . . . . .	14
2.2.5 Image Capture and Analysis . . . . .	16
2.2.6 Phase reconstruction algorithm used in DPI data . . . . .	17
<b>3 Liquid Jet Polishing (LJP) Technique</b>	<b>21</b>
3.1 Introduction . . . . .	21
3.2 Optical polishing . . . . .	22
3.2.1 Ultrasonic Assisted Polishing . . . . .	22
3.2.2 Bonnet polishing . . . . .	23
3.2.3 Magneto rheological polishing . . . . .	24
3.2.4 Liquid jet polishing . . . . .	24
3.3 Development of prototype Liquid jet polishing . . . . .	25
3.3.1 Calculated volume of Slurry Tank . . . . .	26

3.3.2	CAD design of Slurry Tank . . . . .	27
3.3.3	Stirring motor . . . . .	28
3.3.4	Pressure gauge . . . . .	29
3.3.5	Goniometer . . . . .	29
3.3.6	Stand off distance (SOD) . . . . .	30
3.3.7	Nozzle size and shape . . . . .	31
3.3.8	Motorized stage . . . . .	32
3.3.9	Recycle Tub . . . . .	33
3.3.10	Integration Setup of Liquid Jet Polishing :- . . . . .	34
<b>4</b>	<b>Results and discussion</b>	<b>37</b>
4.1	Measurement by using Fizeau interferometer . . . . .	37
4.2	Measurement by using Diffraction Phase Imaging . . . . .	39
4.2.1	Calibration of DPI . . . . .	40
4.2.2	Measurement of BK-7 Glass plate polishing by using LJP at various paramter . . . . .	41
<b>5</b>	<b>Conclusions and Future scope</b>	<b>48</b>

# Acronyms

**DPI** Diffraction Phase Imaging

**LJP** Liquid jet polishing

**BS** Beam Splitter

**SLD** Supper luminescent Diode

**CL** Collimated lens

**DOF** Degree of freedom

**FWHM** Full Width at Half Maximum

**LDC** Laser Diode Current

**ROC** Radius of Curvature

**TIR** Total Internal Reflection

**MRF** Magneto Rheological Finishing

**UAP** Ultrasonic Assisted Polishing

# Chapter 1

## Interferometry

### 1.1 Introduction

Interferometry is a robust optical technique based on the interference of electromagnetic waves. When two light waves, emanating from an identical source interfere, their electric fields add up to give a dc part and a spatio-temporally oscillatory part. The latter manifests itself as intensity variation or fringes, that shows the phase information of the two interfering beams [9] across the sample. Interference in light waves was first observed by Thomas Young in 1801, which also debunked the prevalent corpuscular theory of light, and established light as a wave.

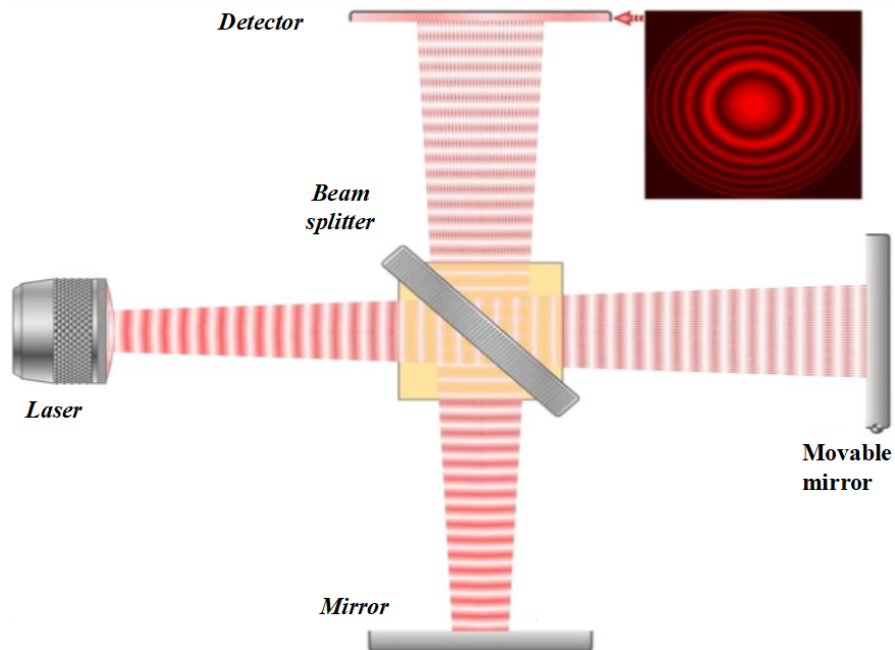


Figure 1.1: Image of interference through interferometry. from ref [17]

Interferometry finds its applications in a vast majority of fields including depth sensing, radar imaging, long distance communications, fine and hyperfine measurements,

surface profiling, etc. The thesis discusses the application of interferometry to measure surface roughness and surface profile [9].

Consider a monochromatic source of wavelength  $\lambda$  incident on the beam-splitter of a Michelson interferometer, having two arms, the arm length difference being  $\Delta z$ . The intensity recorded on the detector will be a sum of individual intensities and a phase dependent term

$$I(x, y) = I_r + I_t + 2\sqrt{I_r I_t} \times \Gamma(\Delta z, \Delta \lambda) \cos(\Delta \phi) \quad (1.1)$$

$$\Delta \phi(x, y) = \frac{2\pi}{\lambda} \times \Delta z(x, y) \quad (1.2)$$

where

- $I(x, y)$ : Interference intensity at point  $(x, y)$  on the detector or camera.
- $I_r$  : Intensity of the reference beam.
- $I_t$  : Intensity of the test (or sample) beam.  $\Delta z$ : Optical path difference between the reference and test beams.
- $\Delta \lambda$ : Spectral width (bandwidth) of the light source. A broader bandwidth means lower coherence length.
- $\cos(\Delta \phi)$ : Represents the cosine of the phase difference between the two beams. This determines whether the interference is constructive or destructive.
- $\Gamma(\Delta z, \Delta \lambda)$  Degree of coherence (also called the coherence function). It depends on the coherence length of the source.

The degree of coherence is important property of the source that defines the quality of the interference fringes [9]. The interference fringes are visible only when the path difference between the two beams is within the coherence length of the source. Therefore, for a longer coherence length source like laser (few cm to few meters), it is easier to get fringes with better contrast. On the other hand low coherent light sources having smaller coherence length (few micrometers), getting interference with bright fringes is difficult. While the interference from the laser is easy to achieve, often it is accompanied with multiple ghost fringes due to multiple optical surfaces involved in the optical system. Further the speckle present in the fringes also affect the measurements.

Low coherence interferometry uses a light source with a broad spectral coverage. The test surface is generally mapped or measured with reference to a reference surface (also known as reference flat, as in the case of most interferometers such as phase

shifting interferometers, lateral shift interferometer, Fizeau interferometer). Owing to the polychromatic nature of the source, the coherence length

$$L_{\text{coh}} \sim \frac{\lambda^2}{\Delta\lambda} \quad (1.3)$$

is smaller. The important advantage of a low coherence source is that, it can be used for optical measurements at different wavelengths in a single scan, which removes the undesired phase noise contributed by the ghost fringes arises due to the interference between two far off surfaces and carries the information only in the region of interest (in other words, the setup is free from noises associated with a narrowband source, such as speckle noise). The phase information obtained from an interferometer (delineated in the subsequent chapters) is susceptible to minuscule changes in optical path length, and hence can be used to measure nanometer (sub-nanometer) changes in length scale in the test and reference surfaces.

The basic setup of an interferometer usually includes a light source, a beam splitter, mirrors or reflective surfaces, and a detector or screen to observe the interference pattern. Mostly, the light beam from the source is split using a beam splitter. One of the beam is used as reference beam while the other beam is sample or object beam. The sample beam interact with the sample under test either in transparent or in reflection mode. The sample beam is then recombines with the reference beam to generate interference pattern. These interference pattern include the signature of sample which can be retrieved using suitable post processing of the interference patterns. The optical device that performs this task is called interferometer. There are different types of optical configurations that perform interferometry. Most common among them are the Michelson and Mach-Zehnder interferometer.

In Michelson Interferometer, which was used in the Michelson-Morley experiment and is still widely used in metrology, vibration analysis, and surface profiling. Other types include the Mach-Zehnder, Fabry-Perot interferometers, each with different configurations and specific applications, these interferometers will be discussed in more detail in below sections.

### 1.1.1 Michelson Interferometer

The Michelson Interferometer is a optical instrument that operates on the principle of light interference. It was invented by Albert A. Einstein and is widely used for measuring extremely small changes in distance, optical path length, or refractive index [5]. When light from the source strikes the beam splitter, it is divided into two beams that



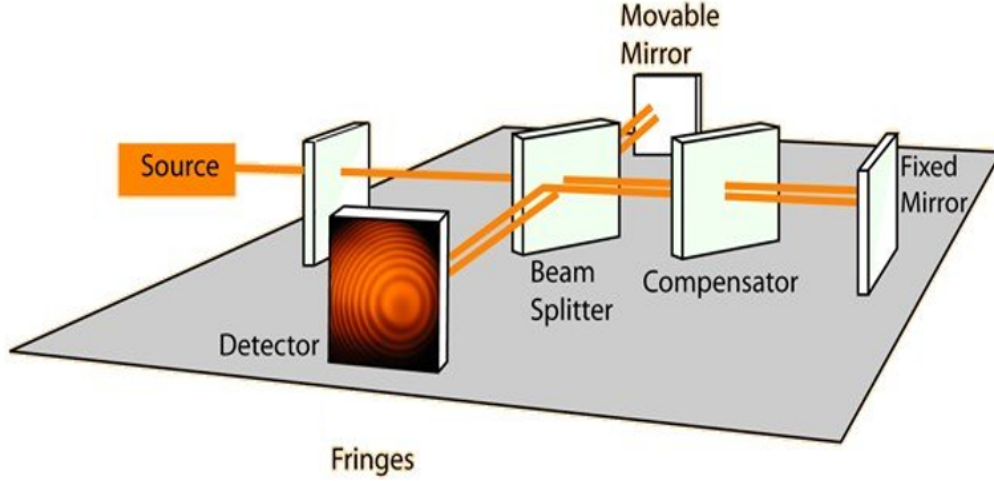


Figure 1.2: Image of Michelson-interferometer adapted from ref [15]

travel along perpendicular paths toward the mirrors. These beams are reflected back to the beam splitter, where they recombine and create an interference pattern, usually observed as alternating bright and dark fringes on the screen. The nature of this pattern depends on the difference in the optical paths traveled by the two beams. If one mirror moves slightly, even by a fraction of a wavelength of light, it causes a shift in the interference fringes, allowing precise measurement of small displacements.

### 1.1.2 Fabry–Perot interferometer

This interferometer makes use of multiple reflections between two closely spaced partially silvered surfaces. Part of the light is transmitted each time the light reaches the second surface, resulting in multiple offset beams which can interfere with each other [10]. The large number of interfering rays produces an interferometer with extremely high resolution, somewhat like the multiple slits of a diffraction grating increase its resolution

#### Fabry-Perot Resolution

A high-resolution interferometer, the Fabry-Perot Interferometer has a resonance of

$$\frac{\lambda}{\Delta\lambda} = \frac{m \times \pi \times \sqrt{r}}{1 - r} \quad (1.4)$$

$m$  = order of interference  $\approx 2d/\lambda$  for small angles.

$r$  = reflection of etalon surface

which means that the least separation of two spectral lines is given by

$$\delta\lambda = \frac{\lambda \times (1 - r)}{m\pi\sqrt{r}} \quad (1.5)$$

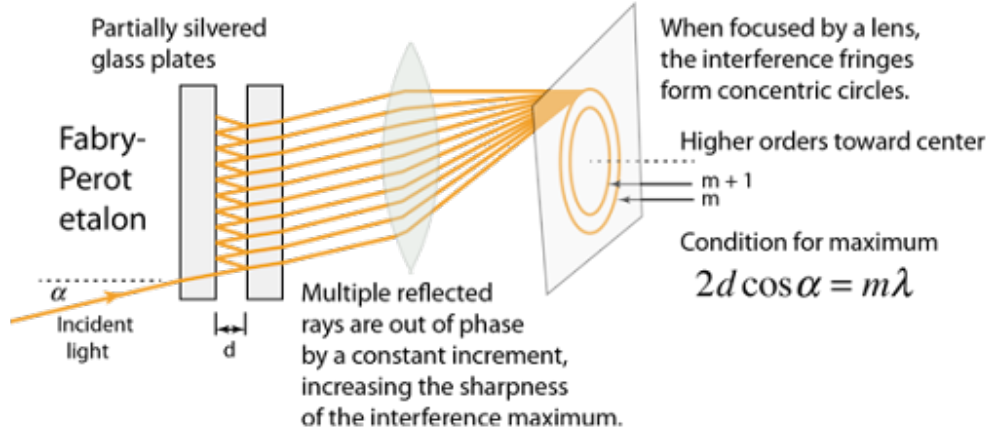


Figure 1.3: Image of Fabry–Perot interferometer adapted from ref [10]

This separation means that the two wavelengths satisfy the Rayleigh criterion. The interferometer can also be characterized by its free spectral range, the change in wavelength necessary to shift the fringe system by one fringe:

$$\delta\lambda = \frac{\lambda^2}{2d} \quad (1.6)$$

### 1.1.3 Coherence Interferometer

A coherent light source, such as a laser, emits light waves that are highly correlated in phase and have a very narrow spectral bandwidth. This means the emitted light has a long coherence length, often spanning several meters or more, depending on the laser type.

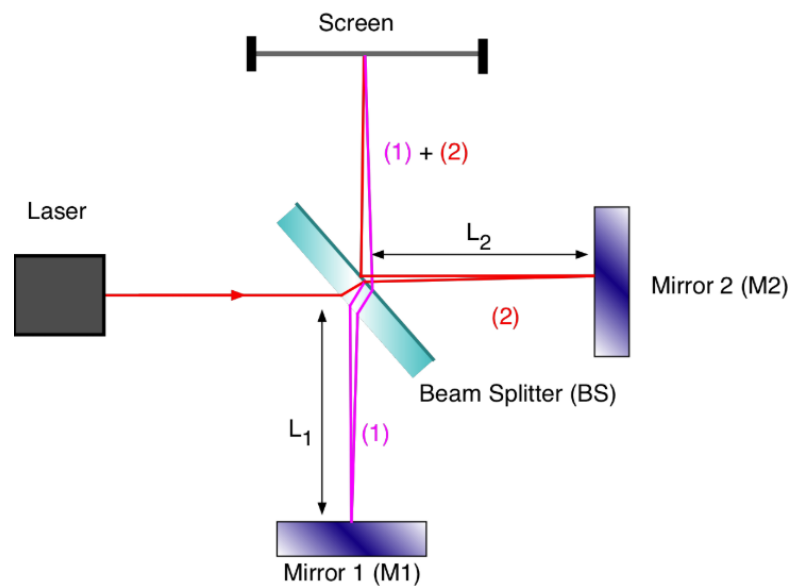


Figure 1.4: Image of Laser-interferometer adapted from ref [12]

Coherent light maintains a fixed phase relationship both temporally and spatially, which makes it ideal for traditional interferometric techniques such as Michelson, Mach–Zehnder, and Fizeau interferometry. In laser interferometry, the coherence of the light allows for stable and high-contrast interference fringes, even when the optical path difference between the test and reference arms is relatively large. This property is especially useful in applications where large-scale or bulk measurements are required. However, coherent sources also come with certain limitations: **Speckle Noise:** The high coherence can lead to speckle patterns, especially when reflecting from rough surfaces, which can degrade measurement accuracy. **Multiple Reflections:** Lasers can produce unwanted interference from multiple surface reflections within the optical system, which may introduce artifacts or noise.

**Limited Spectral Information:** Since the source is monochromatic, it lacks the ability to provide depth-resolved or spectrally-resolved information, which is essential in applications like Optical Coherence Tomography (OCT).

Despite these challenges, laser sources are still widely used due to their high intensity, directional beam, and phase stability. They are particularly effective in applications where high fringe visibility and large measurement ranges are required.

#### 1.1.4 Low Coherence Interferometer

Low Coherence Interferometry (LCI) uses a light source with a broad range of wavelengths, also known as a polychromatic source. In this technique, the surface being tested is compared against a reference surface commonly called a reference flat similar to what is used in interferometers like phase-shifting, lateral shift, or Fizeau interferometers.

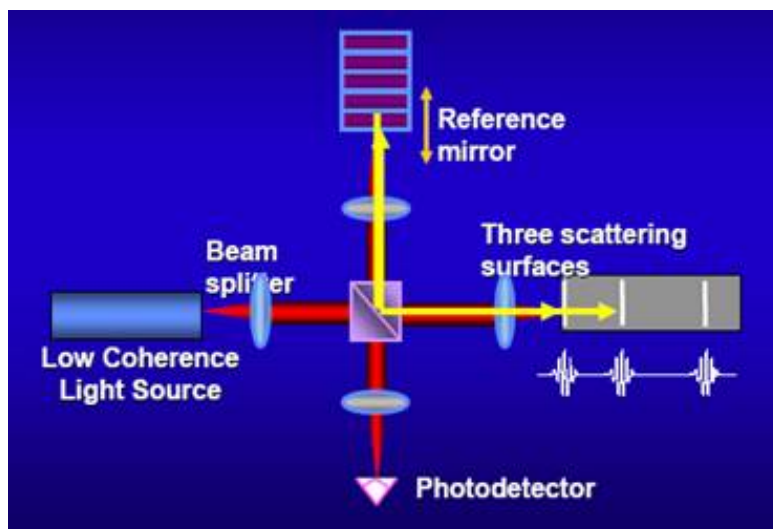


Figure 1.5: Image of Low Coherence Interferometer from ref [13]

Due to the wide spectral bandwidth of the source, the coherence length is significantly reduced. This short coherence length is a key feature of LCI and gives the method its name. Low coherence sources offer several advantages: they enable optical measurements at multiple wavelengths in a single scan [18]. They eliminate unwanted interference from reflections between distant surfaces, reducing phase noise. They provide high sensitivity only within the region of interest, minimizing noise such as speckle that is common in narrow band (single-wavelength) sources. As a result, the phase information captured using low coherence interferometry is highly sensitive to very small changes in the optical path length. This makes the technique suitable for measuring extremely small variations—down to nanometer or even sub-nanometer levels—on both the test and reference surfaces. The light source used in LCI is special. It is a low coherence light source, which means its light waves only stay in sync for a very short distance. Because of this, interference only happens when the two paths are almost exactly the same length. This makes LCI extremely precise, often able to detect differences in depth on the scale of micrometer level.

### **1.1.5 Application of low coherence interferometry**

Interferometry finds applications in a wide range of fields such as optical testing, astronomy, fiber optics, biological imaging, and even in detecting gravitational waves (as seen in the LIGO project). It is also widely used in test surface flatness, material deformation, or mechanical vibration measurement [9]. As well as its use in metrology measurement with high precision level, which is discussed in details as follows.

Interferometry is a technique used in metrology to measure very small distances, surface irregularities, and changes in physical properties with extremely high accuracy. It works by using the principle of interference of light waves—when two light beams combine, they create a pattern that can be analyzed to determine tiny surface structure. This method is especially useful in calibrating precision instruments, testing optical components, and ensuring quality control in manufacturing. Because of its non-contact nature and ability to detect changes on the nanometer scale, interferometry is widely used in advanced research and industrial applications, making it an essential tool in modern metrology.

As an example, a Diffraction Phase Imaging (DPI) system based on interferometry is used for surface profiling. More details about DPI will be discussed in the next chapter.

# Chapter 2

## Diffraction Phase Imaging (DPI) Technique

### 2.1 Introduction

Diffraction Phase Imaging (DPI) is an optical imaging technique that utilizes the principles of diffraction and interference of light to create high-resolution images of transparent samples [4]. The information about the small variation of thickness or the refractive index of the samples is encoded in the interference fringes. These interference fringes facilitates the retrial of the phase changes across the sample. In a DPI system, when an incident light beam interacts with a sample, it gets scattered from the surface-features and induce a phase shift relative to the unaltered or un-scattered reference wave[4]. To measure this small phase variation of the sample, DPI involves a grating that diffracts light into zero and +1 order [19]. The zero order light is passed through a pin hole to filter out the high spatial frequency light generated due to the sample. This act as the reference wave and interfere with the +1 order diffracted light on the charge coupled device (CCD) sensor. As both the sample and reference light are originated from the same sample and both travel adjascent to each other, the system behaves like common path Mach-Zehnder interferometer. The phase shift due to sample is embedded in the intensity variations captured by a camera as an interferogram. Through analysis of these interference patterns, DPI enables the reconstruction of phase maps with high precision down to nanometer scale.

One of the primary challenges in achieving high-sensitivity quantitative phase imaging (QPI) is the presence of phase noise, which arises from mechanical vibrations and air disturbances—issues that commonly affect interferometric systems [4]. DPI, being a common-path technique, inherently less sensitive to ambiance noise. Unlike White light interferometry that requires multiple measurements, DPI typically employs an

off-axis interferometric geometry. The reference wave and the object waves passed through sample are made to interfere at a small angle to each other on the camera sensor. This angular separation spatially encodes the phase information of the sample as high-frequency interference fringes across the entire field of view in a single shot. The spatial frequency of these fringes is directly related to the angle between the two interfering beams. The single shot imaging feature allows phase imaging at a rate limited only by the imaging speed of the camera.

Furthermore, DPI is a noninvasive, label-free technique that does not require staining or coating of the sample, making it well-suited for a wide range of applications [4]. These include observing various biological specimens, monitoring nano-scale dynamic processes, analyzing semiconductor wet and photochemical etching, studying surface wetting and evaporation, measuring thicknesses of optical coatings and thin films, investigating the self-assembly of nano-structures, assessing material deformation, and identifying defects in semiconductor wafers etc.

The DPI system is capable of functioning in both transmission and reflection modes, making it suitable for imaging both transparent and opaque specimens. The following section is dedicated to describe the working principles of the DPI operation, both in transmission and reflection configurations.

### 2.1.1 Transmission mode Diffraction Phase Imaging

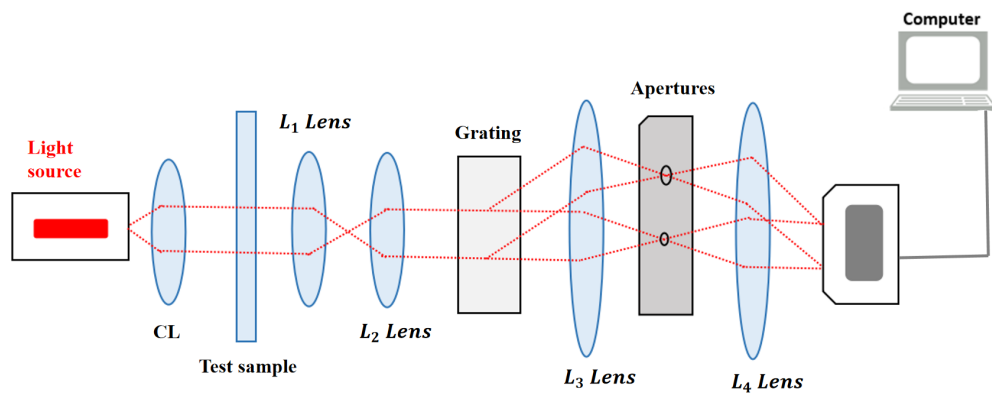


Figure 2.1: Schematic of DPI set up in transmission configuration

Figure (2.1) shows a transmission mode DPI set up which is suitable for measurement of the surface topography of transparent or less reflective optical surfaces. The first pair of lenses used in this system serves as an optical microscope which produces a magnified or de-magnified image of a test sample on a grating, placed at the image

plane of the microscope. The transmission grating produces multiple copies of the image by diffraction at different angles, among which only the  $0^{th}$  and  $1^{st}$  orders are taken to create the final interferogram. After the grating another pair of lenses are used (in  $4f$  configuration) to create the interference. A spatial filter (mask) is placed in the Fourier plane (i.e. focal plane of the third lens) which allows the  $1^{st}$  order to pass and the  $0^{th}$  order is filtered down using a small pinhole to carry only the dc part. After the Fourier transform by the fourth lens, this spatially filtered field becomes a uniform plane wave which serves as a reference, whereas the unfiltered  $1^{st}$  order beam carries all the surface information. These two fields interfere at the final image plane on the detector and phase information is extracted from the recorded interferogram data.

A detailed description of the optical components used in the transmission mode DPI system and their specifications are discussed in the beginning of Section 2.2, prior to the development of DPI system in transmission mode.

### 2.1.2 Reflection mode Diffraction Phase Imaging

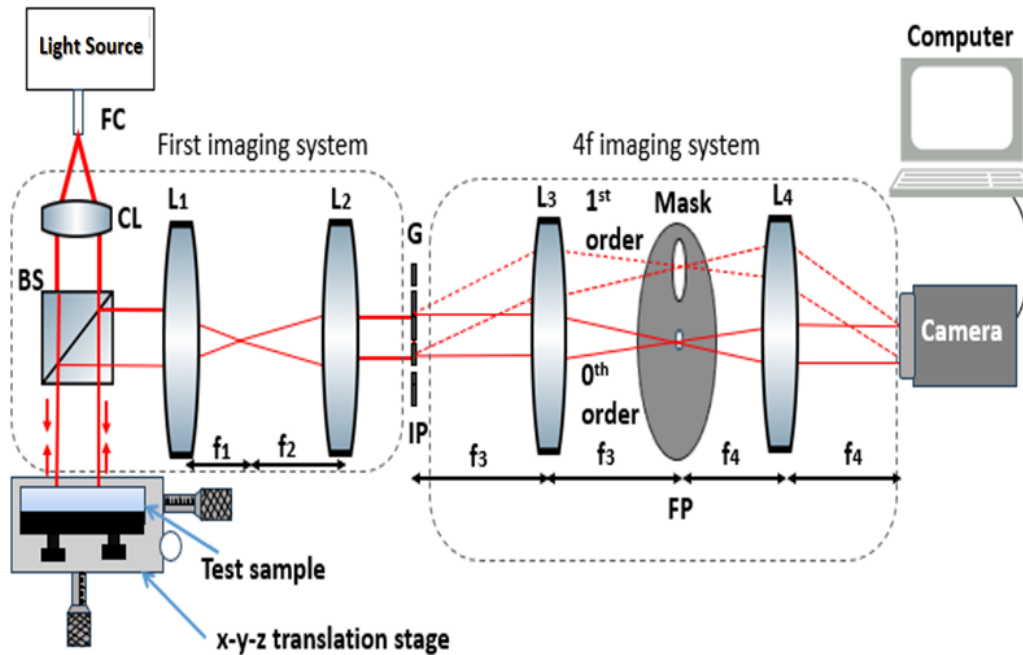


Figure 2.2: Schematic of DPI set up in reflection configuration [19]

Figure (2.2) shows the schematic of the DPI setup. The collimated beam passes through a beam-splitter (BS) and after transmission, one part of the beam is incident on the reflective test sample. The reflected beam from the sample enters into the first imaging system (microscope). The rest of the setup remains identical to the configuration



previously outlined for transmission mode DPI.

This configuration is generally used to characterize and measure the surface shape or roughness of non-transparent or opaque but highly reflective optical surfaces.

In the next section, the development of the prototype transmission mode DPI system is discussed.

## 2.2 Development of prototype transmission mode DPI system

Initially, as the LJP system was not ready, the DPI set up was developed in reflection mode to image the available reflecting surfaces like mirrors. Figure (2.3) and (2.4) show the photograph and CAD design respectively of the reflection mode DPI system. The developed DPI setup used a diode Laser (Coherent Visible Laser Module, VMB2.3-4L, emission wavelength at 635 nm) as the light source. The collimated beam of light was first passed through an intensity filter to control its power and it is incident on a beam-splitter (BS). After transmission through the BS, one part of the beam is incident on the reflective test sample. The reflected beam from the sample enters into an imaging system consisting of two convex lenses  $L_1$  and  $L_2$  having focal lengths of  $f_1$  and  $f_2$  respectively. On the imaging plane, a transmission grating with period 100 lines/mm is placed which diffracts the incident collimated beam. Both the beams are then passed through a convex lens  $L_3$  and a mask is placed at the focal plane of  $L_3$ , which allows the  $0^{th}$  order and  $1^{st}$  orders beams only for phase imaging.

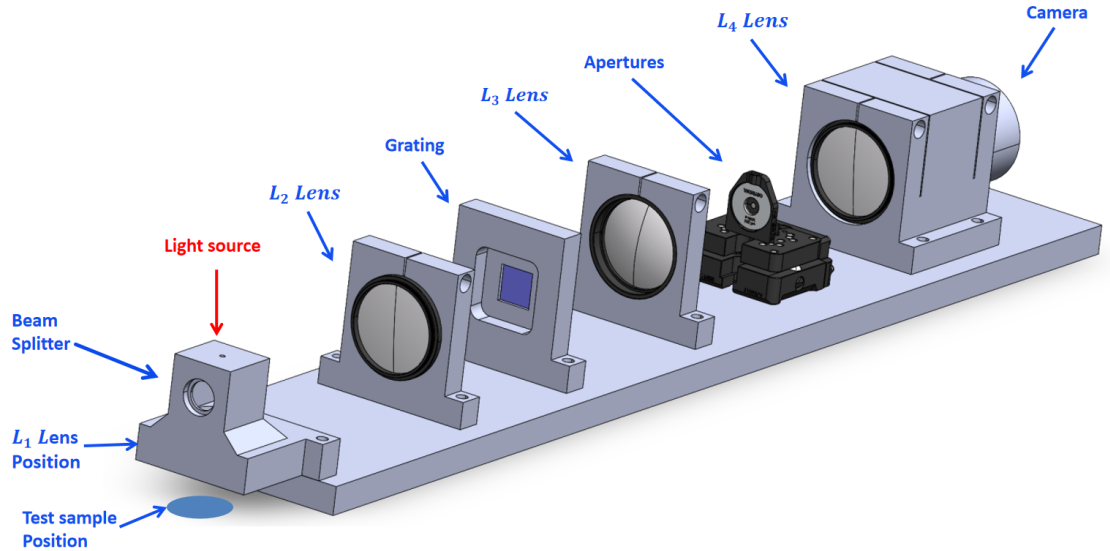


Figure 2.3: CAD design of DPI set-up in reflection configuration

A pinhole at the center of the mask performs a low-pass filtering to the  $0^{th}$  order beam and thus produces a relatively flat wavefront used as the reference. The  $1^{st}$  order

beam remains unaltered and hence its wavefront carries the phase information of the test surface.

The two beams interfere when they are collimated and converge at the focal plane of the fourth lens  $L_4$ . A camera (Pi-Cam-V2, 2000, 3000 pixels, 16-bit,  $1.22 \times 1.22 \mu\text{m}^2$  pixel size) is placed at this focal plane to record the interference signal which is used to extract the phase-map of the test surface.

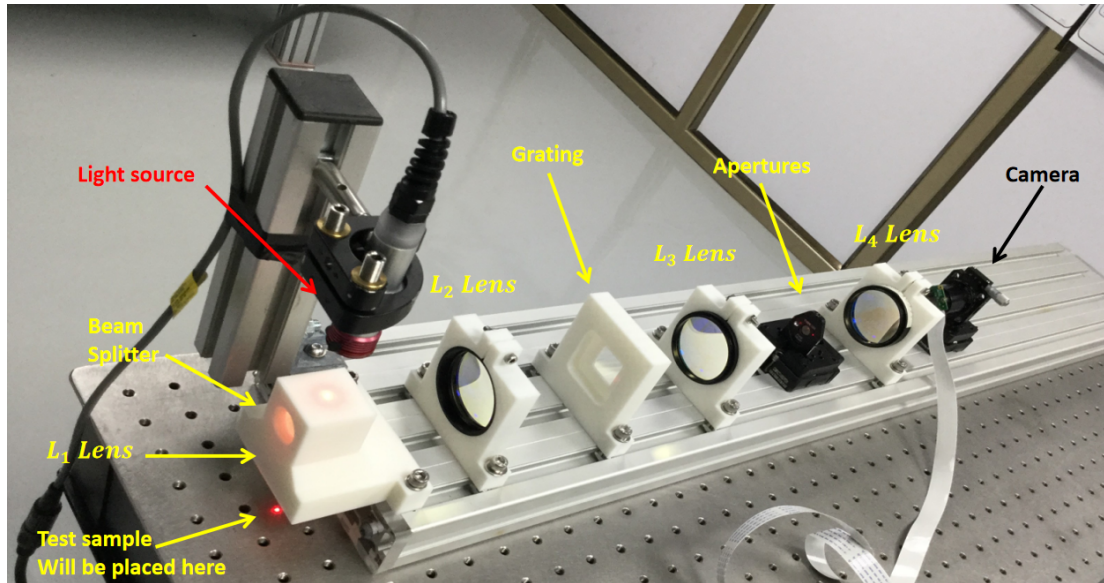


Figure 2.4: Image of DPI set up in reflection mode in RRCAT laboratory

Later the LJP system was developed and the actual transparent samples were available for imaging. However due to transparent nature of sample signal strength was low in reflection mode DPI hence for better signal strength the transmission mode DPI setup was developed. Once the system was fully assembled, experimental work was carried out using this setup. Figure (2.5) shows the photograph of the developed transmission mode DPI system.

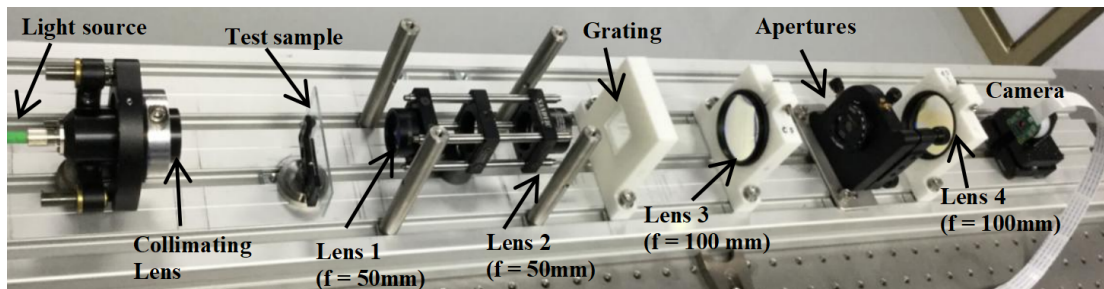


Figure 2.5: Image of DPI set up in transmission configuration in RRCAT laboratory

In our experiment, we used a diffraction phase imaging (DPI) setup to measure the

surface topography of the polished BK-7 glass plate. The optical system was designed to capture phase information with high sensitivity and resolution. The major components and their functions are described below:

### 2.2.1 Light Source and Collimation



Figure 2.6: Image of Super luminescent Diode (SLD) used in our experiment

The light source used in the setup is a Super luminescent Diode (SLD), which is connected to a single-mode optical fiber. This type of light source provides spatially coherent but temporally low-coherence light. This combination helps to reduce speckle noise while still giving good image contrast, making it ideal for high-quality imaging. The light coming out of the single-mode fiber is divergent, so a lens with a 50 mm focal length is used to collimate the beam. Collimation ensures that the light rays are parallel, providing even and uniform illumination of the sample surface.

### 2.2.2 Sample Illumination and first 4f Imaging System

The collimated light beam illuminates the sample, which is placed at the front focal plane of the first lens in a 4f imaging system. This 4f system is made up of two identical 50 mm achromatic lenses. The first lens captures the light reflected from the sample and focuses it to form an intermediate image. The second lens then relays this image onto a diffraction grating placed at the image plane of the first 4f system. The purpose of this 4f setup is to project a high-quality image of the sample onto the grating, preserving phase information with minimal aberrations.

### 2.2.3 Diffraction Grating

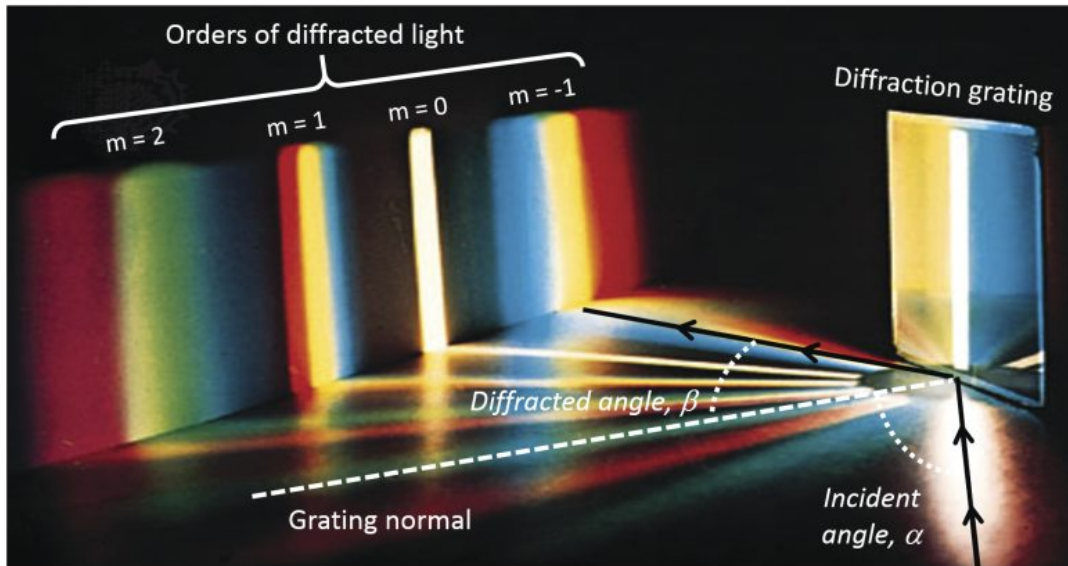


Figure 2.7: Image of transmission grating, adapted from ref [14]

At the image plane of the first 4f system, a transmission diffraction grating is placed which is shown in Figure (2.7). This grating splits the image into multiple diffraction orders ( $0^{th}$ ,  $\pm 1^{st}$ , etc.). To perform phase-shifting interferometry, it is essential to isolate one of the diffracted orders to interfere with a reference beam. This is achieved using another 4f imaging system.

### 2.2.4 Second 4f imaging system and masking using pinhole

A second 4f system, composed of two achromatic lenses with 100 mm focal lengths, is used to relay the image of the grating onto a CCD camera. This system has a total magnification of 1, ensuring that the size of the final image on the CCD is the same as that of the sample. Between the two lenses of this 4f system, a spatial filter (mask) is placed at the Fourier plane. This mask blocks the high spatial frequency signal present in the zero-order beam and makes the light as undeviated or reference light. The mask also allows the  $+1^{st}$  diffracted order to pass through as it is, and blocks other higher-order diffraction terms. This filtering process ensures that the image formed on the CCD consists of interference between the reference ( $0^{th}$  order) and sample-modulated beams ( $1^{st}$  order) only.



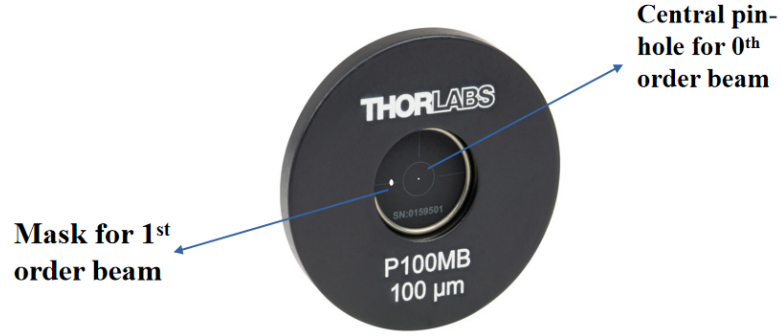


Figure 2.8: Image of Pin hole and mask used in our DPI set up

Figure (2.9) and (2.10) shows the propagation of light using Zemax software for zeroth order and 1<sup>st</sup> order of diffracted light from the transmission grating.

#### (a) First order

1<sup>st</sup> Order using as getting information of test sample how much roughness on test sample.

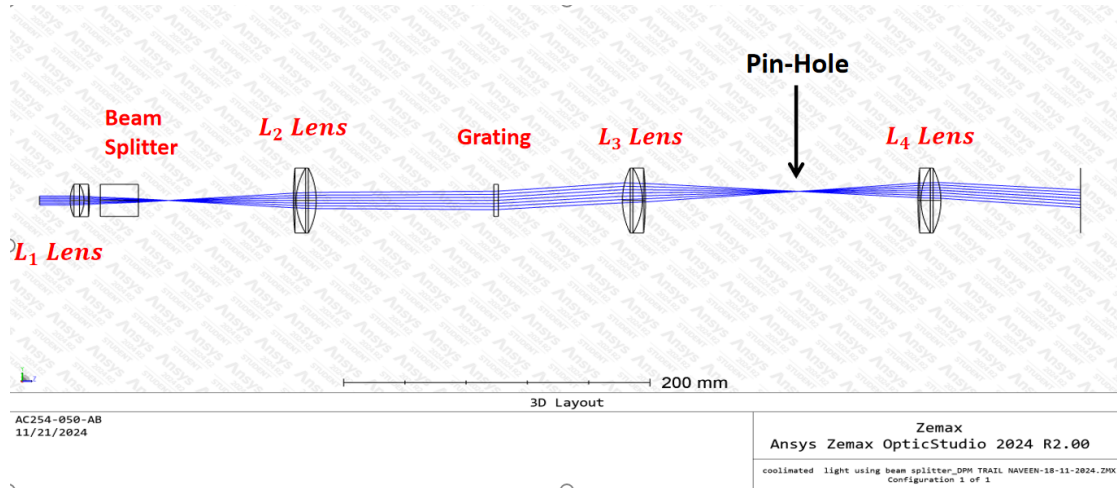


Figure 2.9: Ray tracing by using Zemax Design for 1<sup>st</sup> order

#### (b) Zeroth Order

0<sup>th</sup> Order beam using as reference beam which is comparing with 1<sup>st</sup> order beam then we are getting information of test sample .

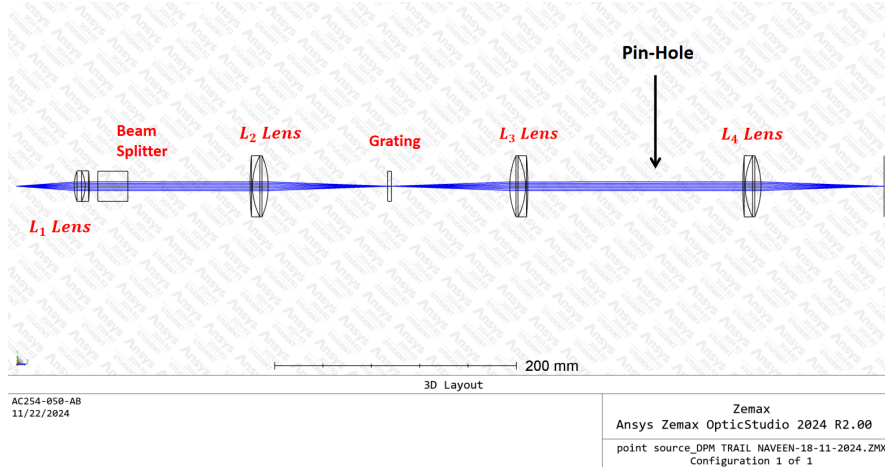


Figure 2.10: Ray tracing by using Zemax Design for  $0^{th}$  order

### (c) Calculation of focused spot diameter ( $FS_{dia}$ ) [20]

$$FS_{dia} = \frac{4f\lambda}{\pi D} \quad (2.1)$$

$$FS_{dia} = \frac{4 \times 100 \times 10^{-3} \times 840 \times 10^{-9}}{3.14 \times 2.5 \times 10^{-3}} \quad (2.2)$$

$$FS_{dia} \approx 40 \mu m \quad (2.3)$$

which is smaller than the central pinhole diameter ( $100 \mu m$ ) used in our experiment, ensuring no significant intensity loss of the on-axis beam while passing through the pinhole.

### 2.2.5 Image Capture and Analysis

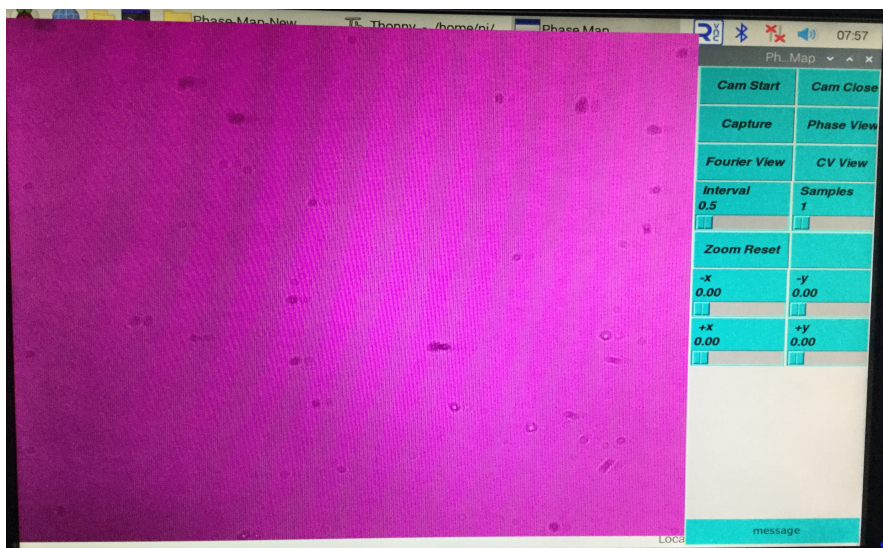


Figure 2.11: Image of the interface for live-monitoring, recording and analyzing of interferogram

A CCD camera placed on the imaging plane of 4f lens system captures the interference image. The interference image carries both amplitude and phase information of the sample. The phase information of the sample can be obtained by processing of the interference fringe signal using Fourier phase retrieval algorithm. Figure (2.11) shows the photograph of the screen showing the interference image of the sample captured by the Raspberry Pi-cam.

### 2.2.6 Phase reconstruction algorithm used in DPI data

In the following, a computational phase-extraction method from the recorded fringe-pattern is discussed which was first proposed by M. Takeda et al. [21].

Mathematically an interference signal can be expressed as [21],

$$g(x,y) = a(x,y) + c(x,y) e^{i(2\pi f_0 x + \phi(x,y))} + c.c. \quad (2.4)$$

where  $f_0$  is the spatial carrier frequency along x-direction and  $c.c$  indicates the complex conjugate.

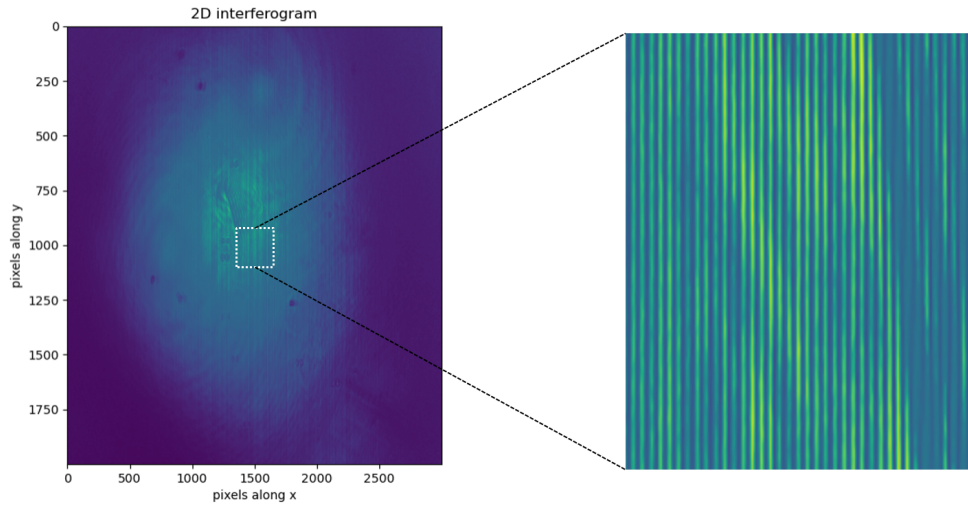


Figure 2.12: Image of a 2D interferogram (left) and the fringes shown in the magnified portion (right)

Applying a fast Fourier transform (FFT) with respect to  $x$ , the spectral components become:

$$G(f,y) = A(f,y) + C(f - f_0,y) + C^*(f + f_0,y), \quad (2.5)$$

The FFT separates the spectral components. One of the sidebands, such as  $C(f - f_0,y)$ , is shifted to the origin by  $f_0$  in the frequency domain to isolate  $C(f,y)$ . This



effectively removes the dc part.

To extract the complex field  $c(x,y)$ , the inverse FFT is applied to  $C(f,y)$ . Finally, the phase  $\phi(x,y)$  is obtained by computing the argument of it. Similar steps can be extended for a 2D array of the interferogram.

The 2D interferograms are initially captured in BGR (Blue-Green-Red) image format, which is the default output format for many digital imaging sensors. A typical interferogram is shown in Figure (2.12).

To make further processing to extract the intensity values needed for phase reconstruction, the captured BGR images are converted to grayscale representing brightness of each pixel. Use of a grayscale image is suitable for Fourier analysis to retrieve phase information [21].

Following grayscale conversion, Takeda's algorithm is applied as discussed before. The entire procedures is written in compact form as follows:

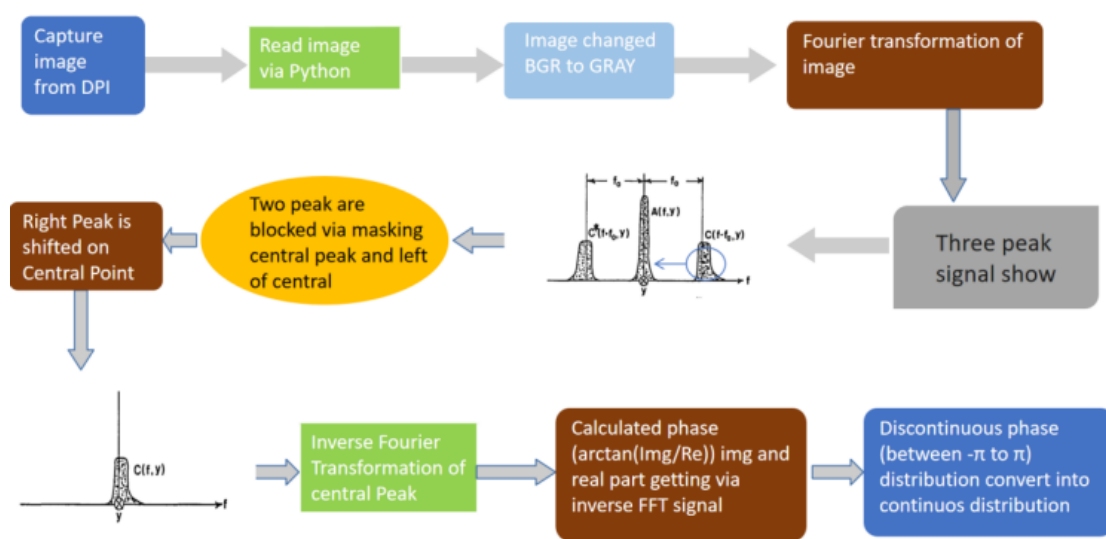


Figure 2.13: Flow chat of DPI algorithm for phase extraction

The final argument is a wrapped phase image, where phase values are confined within the interval  $-\pi$  to  $+\pi$  which is then unwrapped to obtain the 2D phase map of the sample.

For a typical 2D interferogram, after applying Fourier transform (FT), shifting of the 1st order back to the center and inverse FT, the result becomes:

$$2|U_{\text{ref}}| \cdot |U_{\text{sample}}(x,y)| \cdot \exp(i\phi(x,y)) \quad (2.6)$$

Without any sample (only BG), we obtain after image-processing :

$$2|U_{\text{ref}}| \cdot |U_{\text{sample}}(x,y)| \cdot \exp(i[\phi_{bg}(x,y) + \phi_n(x,y)]) \quad (2.7)$$

With sample, we obtain after image-processing :

$$2|U_{\text{ref}}| \cdot |U_{\text{sample}}(x,y)| \cdot \exp(i[\Delta\phi(x,y)\phi_{bg}(x,y) + \phi_n(x,y)]) \quad (2.8)$$

where:

- $\Delta\phi(x,y)$ : Phase of Sample under tested
- $\phi_{bg}(x,y)$  : Phase of the background (BG)
- $\phi_n(x,y)$  : Phase induced by noise

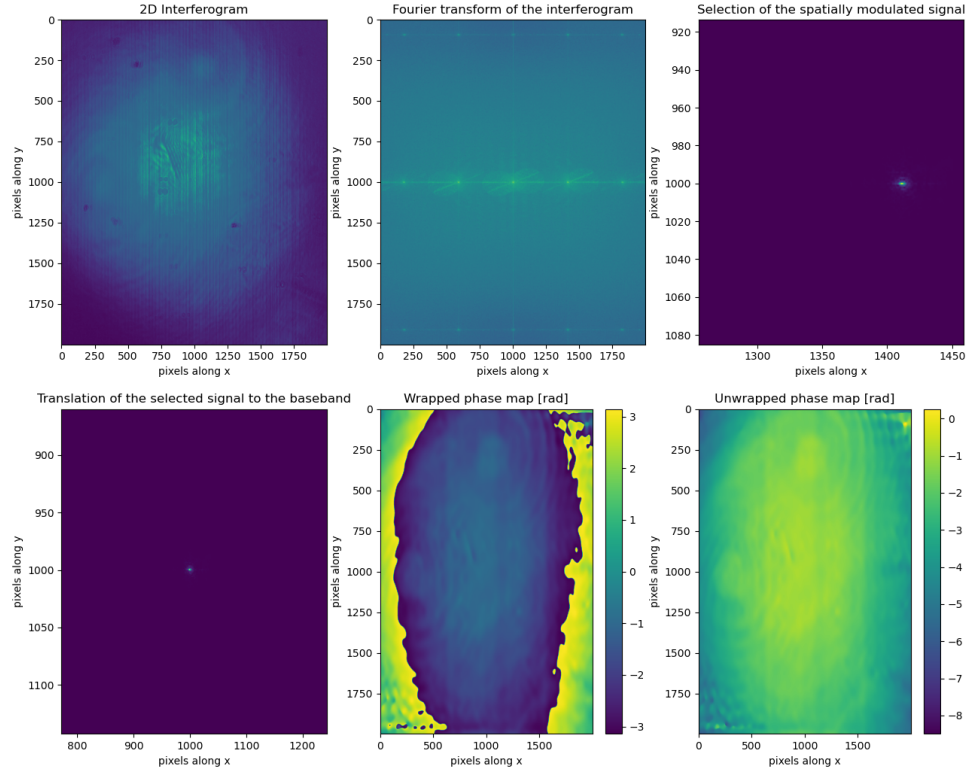


Figure 2.14: Analysis of a 2D interferogram by Takeda's method.

The phase-maps can be obtained from equation (2.6) and equation (2.7) by taking the argument and unwrap them and then subtract to obtain the unwrapped phase map (in radian) of the sample.

This intensity pattern can be contaminated by dirt or defects on optical components or alignment of the system. It also include the phase change arises at the optical components. This can be corrected by background subtraction. For this, a background image

is captured without any sample, and finally unwrapped phase of the background image is subtracted from the unwrapped phase image of sample under test (SUT).

To obtain the actual physical phase distribution, a phase unwrapping algorithm is applied. This algorithm converts the wrapped phase map, which contains sudden jumps or discontinuities, into a smooth and continuous phase map. The resulting unwrapped phase represents the optical path difference, which can then be used to calculate the step height or thickness variation across the surface of the sample.

An interferogram of the test surface was first captured, revealing visible interference fringes, as shown in the inset image. These fringes indicate surface changes of test sample. After background removal, an unwrapped phase map was obtained, clearly showing localized phase variations due to material removal.

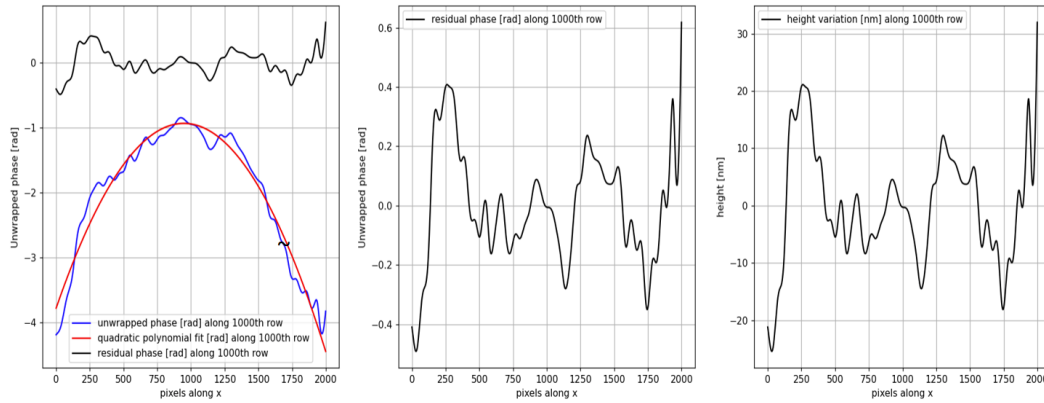


Figure 2.15: Image of Plotted graph variation on scratched mirror

A cross-sectional phase profile was then extracted along the 1000th row of the phase map to analyze the phase change in detail. This profile, shown in radians, highlights the shape and depth of the test sample. Finally, the phase data was converted into height measurements in nanometers, revealing that created maximum depth of approximately  $\approx 40$  nm. This confirms the capability with DPI providing accurate and detailed analysis of the surface topography.

# Chapter 3

## Liquid Jet Polishing (LJP) Technique

### 3.1 Introduction

As we know increasing demand of optical components in high-tech fields like lasers, aerospace, space optics, and precision instruments, the need for surfaces with extremely high smoothness and minimal defects has grown significantly.

Preparing optical materials involves several important stages, and each stage plays a key role in determining the final surface roughness of the component. The process usually starts with cutting and shaping the raw optical material into the desired size and form. This is often done using diamond saws or grinding tools, which can leave the surface relatively rough. There are different stages involved in preparing optical materials that reduce the surface roughness progressively. These stages are briefly described as below:

#### (a) Blank Preparation

This is the initial step where the optical material is roughly cut and shaped. The surface roughness at this stage is less than 10 micrometer. It's mainly for cutting and flattening the raw material.

#### (b) Generation (Shaping)

In this step, the basic shape of the optic (such as curves or flat surfaces) is formed. The surface roughness typically ranges between 1 to 10 micrometer. This stage involves a high material removal rate.

#### (c) Fine Grinding

Here, the surface is smoothed further to prepare it for polishing. The roughness at this stage is around 500 nm, and this is when a more ductile (less brittle) surface finish starts

to appear.

#### (d) Polishing

This final step gives the surface its optical quality finish, with a roughness of less than 10 nm, making it suitable for use in optical applications.

Different Stages	Purpose	Typical Surface Roughness	Notes
Blank Preparation	Rough cut and shape of optical material	$< 10 \mu\text{m}$	Initial Block cutting, flattening
Generation (Shaping)	Form approximate geometry (curves/flats)	$\approx 1\text{-}10 \mu\text{m}$	High removal rate
Fine Grinding	Smooth surface, prepare for polish	$\approx 500\text{nm}$	Ductile finish starts
Polishing	Achieve optical finish and figure	$< 10 \text{ nm}$	Optical quality surface

Figure 3.1: Image of Steps for fabrication of optics

## 3.2 Optical polishing

Ultra-polished optics is important in the field of imaging and precision metrology . It can improve the performance of optical systems by reducing the scattering. There are various techniques to perform ultra- polishing or super smooth polishing such as Ultrasonic Assisted Polishing, Bonnet polishing, Magneto Rheological Finishing (MRF), Liquid Jet Polishing (LJP), etc [22], more details will be discuss in next sections. These techniques remove the surface material to achieve the surface figures in the range of few micrometers to a few nanometers.

### 3.2.1 Ultrasonic Assisted Polishing

Ultrasonic Assisted Polishing (UAP) is a technique where high-frequency ultrasonic vibrations (typically above 20 kHz) are applied to the polishing tool or the workpiece during the polishing process [22]. These vibrations help to reduce friction, improve the movement of abrasive particles, and enhance the material removal rate.

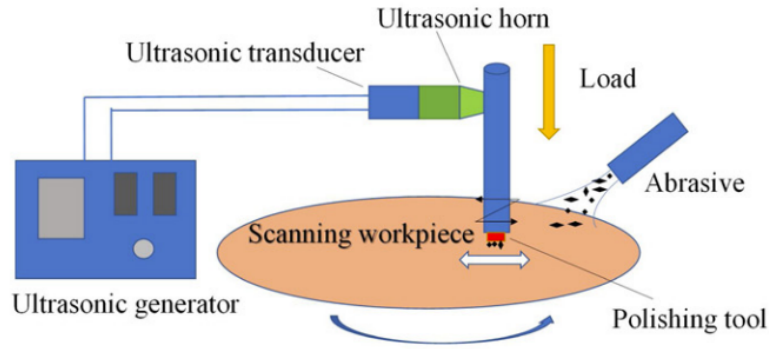


Figure 3.2: Image of ultra sonic polishing from ref [22]

As a result, UAP can produce surfaces with lower roughness, less subsurface damage, and better uniformity, especially on hard and brittle materials like ceramics, glass, and optical components.

### 3.2.2 Bonnet polishing

This technique uses a soft, flexible, and spinning polishing tool called a bonnet covered with polishing cloth or polyurethane. By adjusting the pressure and contact area of the bonnet [22], this method allows accurate and efficient polishing of complex shapes, such as aspheric and freeform optical surfaces. Bonnet polishing is especially valued

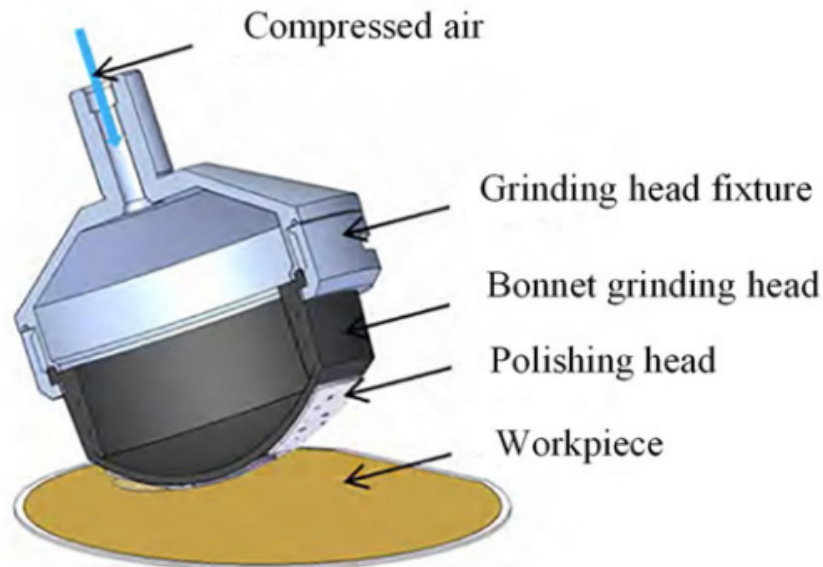


Figure 3.3: Image of bonnet polishing from ref [22]

for its high surface quality, with roughness reaching nanometer levels. The technology is adaptable and has been combined with liquid jet polishing for improved performance on large or low quality surfaces.

### 3.2.3 Magneto rheological polishing

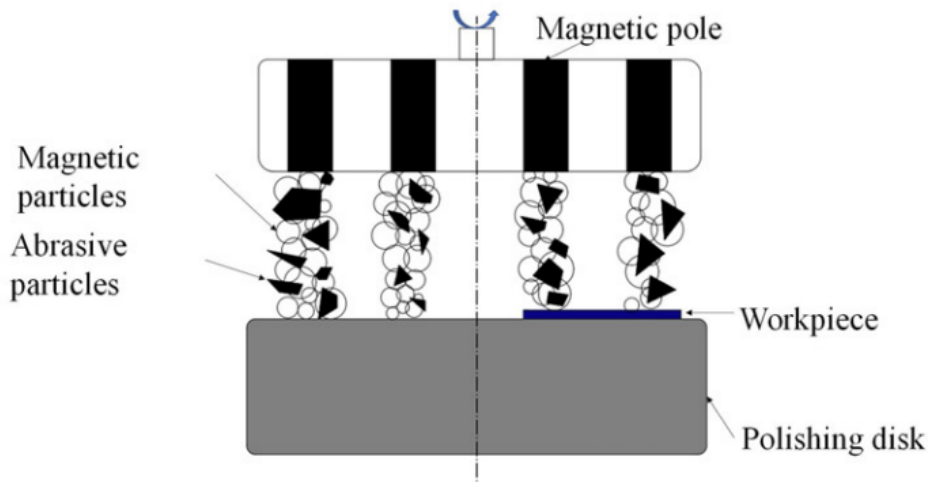


Figure 3.4: Image of Magneto rheological polishing from ref [22]

Magneto-rheological Finishing (MRF) is an advanced polishing technique used to achieve ultra-smooth surfaces on optical components. It uses a special fluid called magneto-rheological fluid, which changes its viscosity when exposed to a magnetic field. This fluid contains abrasive particles that form a ribbon-like polishing zone under the influence of a magnetic field[1]. When the fluid moves across the surface of the workpiece, shear forces generated by the abrasive particles help remove material precisely. MRF offers high precision, low surface roughness, and minimal subsurface damage, making it ideal for polishing complex shapes like a-spherical lenses. Its flexibility, efficiency, and controllability make it one of the most reliable techniques in modern optical manufacturing.

### 3.2.4 Liquid jet polishing

Liquid Jet Polishing is a modern method used to smooth and shape the surfaces of optical components like lenses and mirrors. It uses a stream of liquid mixed with tiny abrasive particles, which is sprayed onto the surface through a small nozzle [6] . This jet gently removes very small amounts of material, helping to fix tiny surface errors or improve smoothness. It is also known as Fluid Jet Polishing.

LJP is useful for polishing complex or delicate shapes that are hard to finish with traditional polishing tools [23]. Because the process does not involve direct contact, it reduces the risk of damaging the optic. It can also achieve very high precise and smooth surface, making it ideal for finishing high-performance optical parts used in telescopes, cameras, lasers, and medical devices.

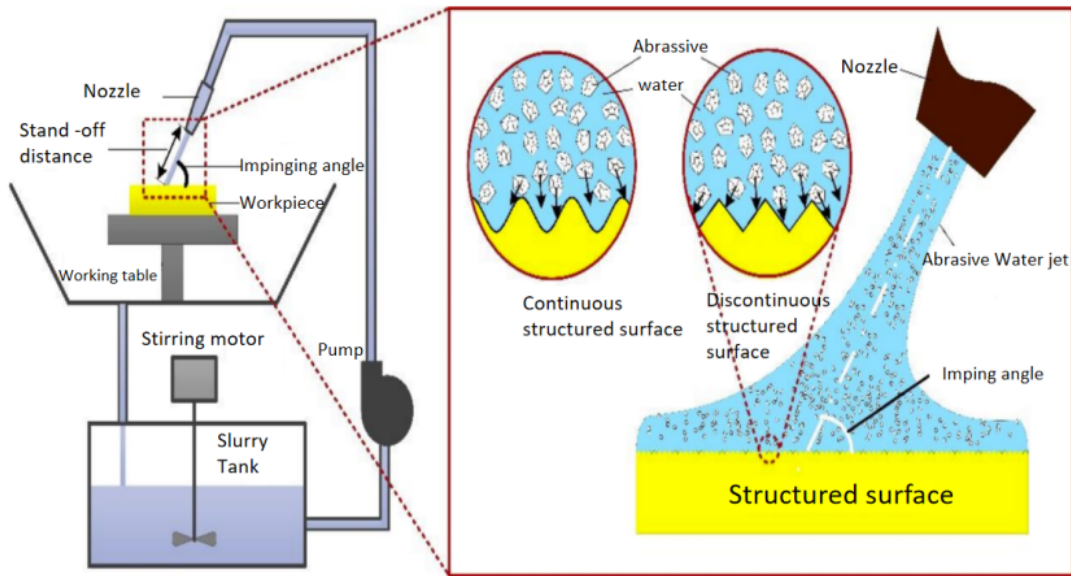


Figure 3.5: Ray diagram of Liquid jet polishing from ref [16]

Each polishing method has its own limitations. Ultrasonic Assisted Polishing (UAP) involves a complex setup with high equipment cost and may cause faster tool wear due to continuous vibrations. It also has limited compatibility with certain materials. Magneto-rheological Finishing (MRF), while precise, is costly due to expensive machines and fluids, requires careful handling, offers a slower material removal rate, and poses environmental challenges in fluid disposal. Bonnet Polishing may lead to uneven edges, tool deformation, and requires precise path control. It is also less suitable for very small or sharply contoured features.

Liquid Jet Polishing (LJP) is highly flexible and can polish complex shapes and freeform surfaces with ease. LJP offers high precision and controlled material removal, resulting in smooth finishes with low subsurface damage. The process is easily adjustable for different materials by tuning parameters like jet pressure and slurry composition. It also allows localized polishing without affecting the entire surface and, depending on the slurry used, can be an environmentally friendly alternative to traditional polishing methods.

Overall, Liquid Jet Polishing is a flexible and accurate technique that helps create extremely smooth and well-shaped optical surfaces.

### 3.3 Development of prototype Liquid jet polishing

Liquid Jet Polishing (LJP) is a precision surface finishing technique that involves several key components such as Slurry tank, Stirring motor, Pressure gauge, Goniometer, Stand



off distance, Nozzle size and shape, Motorized stage, Recycle tub working together to achieve ultra-smooth surfaces without introducing subsurface damage. More details of components will be discuss in next sections:

### 3.3.1 Calculated volume of Slurry Tank

After a thorough out review of research paper, we finalized the decision regarding the slurry tank requirements. Subsequently, the necessary slurry volume was determined, and detailed volume calculations were carried out to design the slurry tank accordingly.

We are calculating flow rate of slurry which is passing through nozzle by using Bernoulli's theorem:-

$$P_1 + \frac{1}{2}\rho v_1^2 + \rho gh_1 = P_2 + \frac{1}{2}\rho v_2^2 + \rho gh_2 \quad (3.1)$$

As we know pressure of atmosphere  $P_2$  and other pressure  $P_1$  which is applied by us :-

$$P_1 = 8 \text{ bar} = 0.8 \text{ MPa}$$

$$P_2 = 1 \text{ bar} = 0.1 \text{ MPa}$$

we know about for normal use Water density  $= \rho = 10^3 \text{ kg/m}^3$

So now putting all value in equation (3.1)

$$8 \times 10^5 + \frac{1}{2} \times 10^3 \times v_1^2 = 1 \times 10^5 + \frac{1}{2} \times 10^3 \times v_2^2 \quad (3.2)$$

As we know initially velocity of water in slurry tank is approx is zero so:-

If we are putting  $v_1 = 0$ , then we are getting value of  $v_2$ :-

$$v_2^2 = \frac{8 \times 10^5 - 1 \times 10^5}{500} \quad (3.3)$$

$$v_2 = 37.4 \text{ m/sec} \quad (3.4)$$

$$V_r = \text{Volume flow rate} = \text{Area} \times v_2$$

$$V_r = \frac{\pi}{4} \times \frac{1}{1000^2} \times 37.4 \quad (3.5)$$

$$V_r = 2.936 \times 10^{-5} \text{ m}^3/\text{s} \quad (3.6)$$

If we are using for 10 min:-

time = 10 min

$$\text{Tank Volume} = V_t = V_r \times t \quad (3.7)$$

$$V_t = 1.761 \times 10 \quad (3.8)$$

$$V_t = 17.61 \text{ litre} \quad (3.9)$$

### 3.3.2 CAD design of Slurry Tank

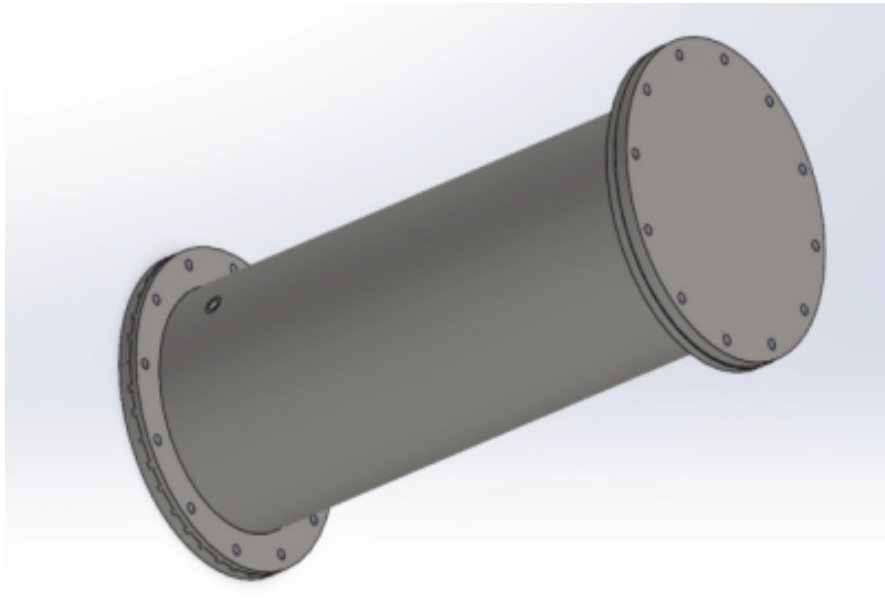


Figure 3.6: Cad design of slurry tank

So finally we are getting volume of tank is 17.61 *litre* for 10 *min* so we have deiced we are use 30 liter volume tank. Now we are moving for tank design part by using of CAD model in solid work software:-

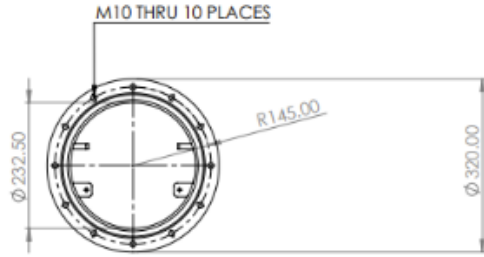


Figure 3.7: Diameter of slurry tank

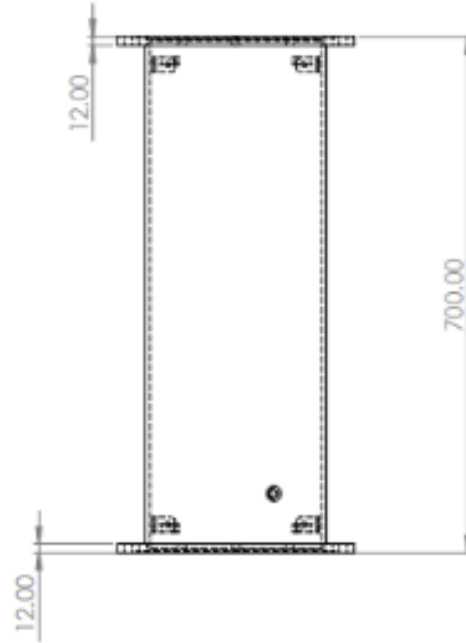


Figure 3.8: Length of slurry tank

### 3.3.3 Stirring motor



Figure 3.9: Image of Stirring motor

In this experiment, a stirring motor is used in the slurry tank to ensure a uniform mixture of water and cerium oxide abrasive particles. During the initial stages of the experiment, the slurry remains well-mixed; however, over time, the cerium oxide tends to settle at the bottom of the tank due to gravity. To maintain a consistent and homogeneous slurry throughout the polishing process, continuous stirring is essential.

### 3.3.4 Pressure gauge

Here, We use a pressure gauge to control the pressure during the polishing process because optimal polishing typically requires a pressure between 6 to 8 bar [7]. Applying pressure beyond this range can deform the substrate and alter its surface, which is undesirable especially since we are working at a precision level in optical polishing. Therefore, delivering pressure in a controlled manner is crucial for achieving the best results in this technique.

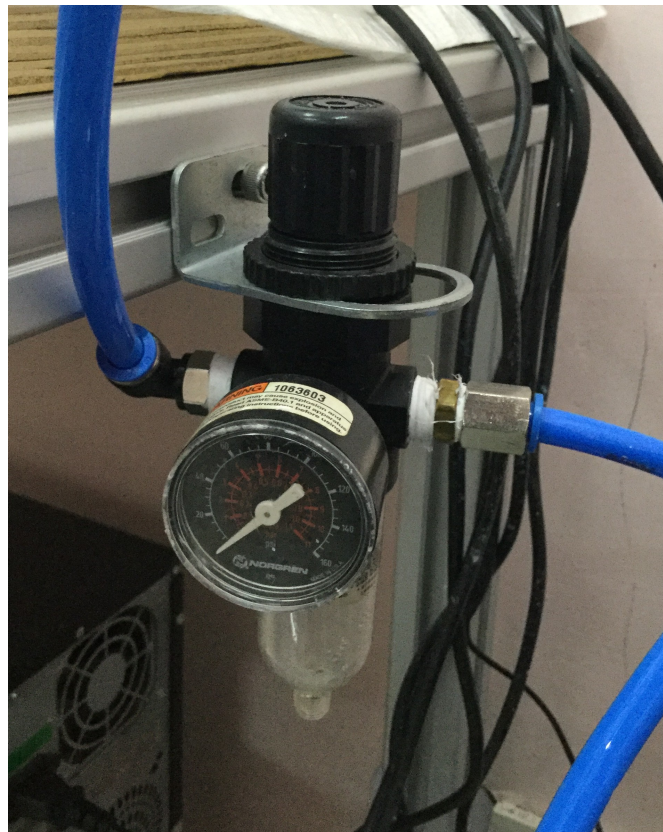


Figure 3.10: Image of pressure gauge

### 3.3.5 Goniometer

In this experiment, a goniometer were used to perform polishing at various angles [23]. The objective was to determine the optimal angle for achieving the best polishing results at the nanometer (nm) scale. During the course of the experiment, it was observed that the angle range between  $45^\circ$  and  $60^\circ$  yielded the most effective polishing outcomes [1]. This demonstrates that the goniometer plays a crucial role in controlling the polishing angle, thereby significantly influencing the surface quality at the nanometer scale.



Figure 3.11: Image of Goniometer

### 3.3.6 Stand off distance (SOD)

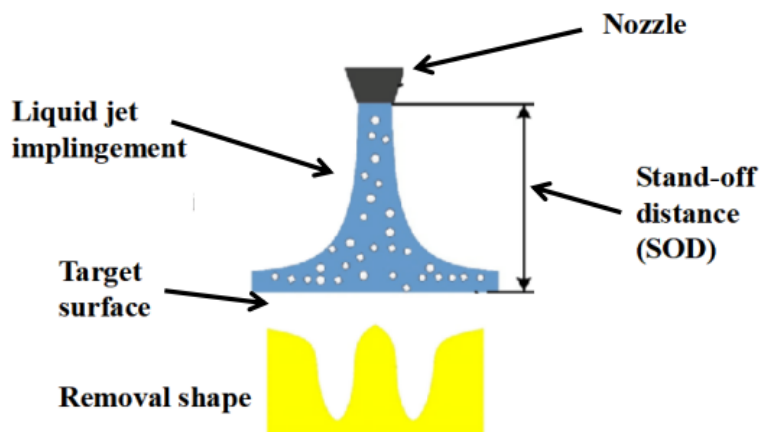


Figure 3.12: Ray diagram of SOD from ref [16]

The stand-off distance plays a critical role in this experiment. During the Liquid jet polishing process, a specific distance is maintained between the nozzle and the optical substrate typically ranging from 5 mm to 7 mm [8].

This distance significantly influences the interaction between the liquid jet and the substrate surface. If the stand-off distance is increased, the impact of the liquid jet on the

substrate is reduced, resulting in less material removal [3]. Conversely, if the nozzle is positioned too close to the substrate, the jet exerts a stronger force, which can lead to excessive material removal and may create large digs or defects on the optical surface. Therefore, careful optimization of the stand-off distance is essential to achieve precise and controlled polishing outcomes.

### 3.3.7 Nozzle size and shape

The size and shape of the nozzle play a crucial role in the liquid jet polishing process [2]. An increase in nozzle diameter results in a larger effective polishing area on the substrate, whereas a decrease in diameter leads to a smaller affected area.

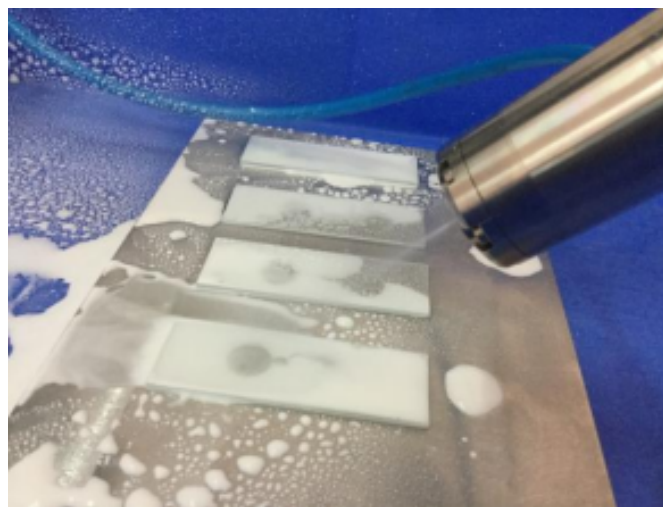


Figure 3.13: Image of 1mm Nozzle

Experimental observations indicate that smaller nozzle diameters are more suitable for precision-level polishing, as they allow for finer control over material removal and surface accuracy.

In addition to size, the shape of the nozzle significantly influences the polishing outcome. While cylindrical nozzles are commonly used, variations such as inward or outward conical shapes can alter the jet's impact profile on the substrate surface. These different nozzle geometries produce distinct polishing effects, making nozzle shape selection an important parameter in optimizing the process for specific material removal rates and surface finish requirements.

#### **Different type of Nozzle:-**

In our experiment, we designed and tested different types of removable nozzles for fluid jet applications. The nozzles used had diameters of 250 microns, 400 microns,



700 microns, and 1 millimeter. Each nozzle size produced different results depending on the experimental conditions.

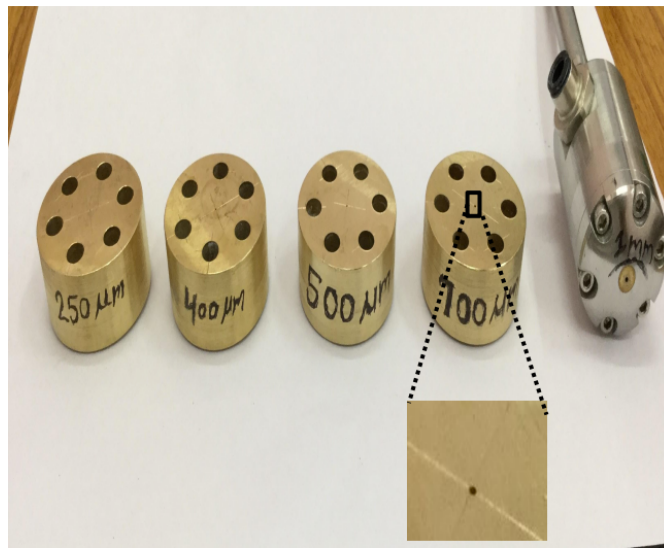


Figure 3.14: Different type nozzle

We observed that when using a mixture of Cerium oxide ( $CeO_2$ ) and distilled water in a 10:1 ratio [8], the mixture could not pass through the 250-micron nozzle properly. This is because the nozzle diameter is too small, making it unsuitable for the given mixture. The particle size and viscosity of the fluid likely contributed to the blockage at such a small diameter nozzle.

### 3.3.8 Motorized stage

In this setup, we are using a motorized stage that moves in both the X and Y directions [23]. This means the substrate (the material being polished) is placed on a platform that can move horizontally in two directions left-right (X-axis) and forward-backward (Y-axis).

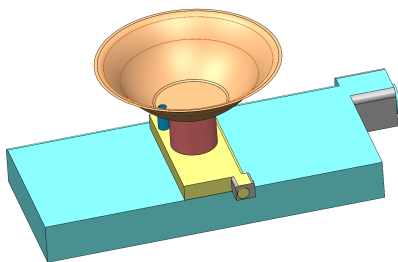


Figure 3.15: Cad design of motorized stage

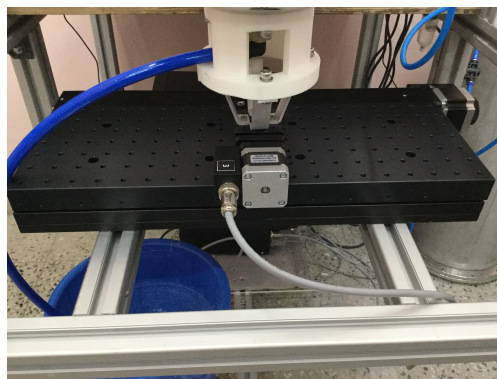


Figure 3.16: Image of Translation stage

As the substrate moves, a scanning process takes place, meaning the polishing tool moves systematically over the surface, covering every point step by step. This ensures uniform polishing across the entire area.

The polishing itself happens through a process called Liquid Jet Polishing (LJP), where a high-speed jet of liquid is directed at the surface to smoothen and refine it. The movement of the stage in both directions allows precise control, ensuring the entire surface is polished evenly.

By scanning in both directions (X and Y), the machine ensures no part of the surface is left untreated, leading to high-quality and consistent polishing results. which is measured by using DPI.

### 3.3.9 Recycle Tub

A recycle tub is used in this experiment to collect the slurry remaining after the polishing process.

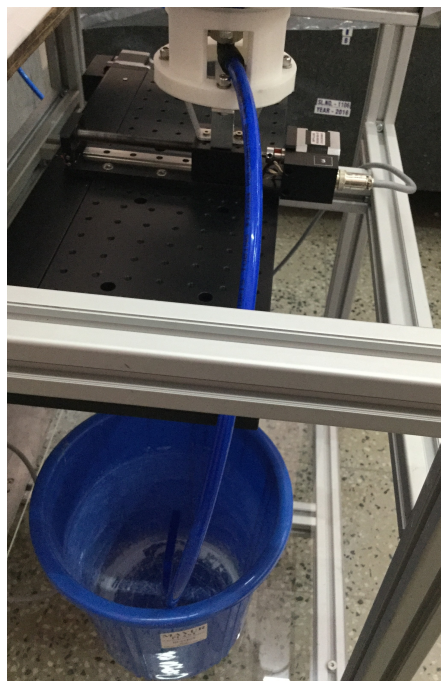


Figure 3.17: Image of Recycle tub

Since a significant portion of the slurry containing both water and cerium oxide particles settles in the tub post-polishing, we decided to reuse it for subsequent experiments.

To ensure safe handling and prevent contamination, the recovered slurry is stored in clean, tightly sealed bottles. These bottles are properly labeled and securely covered to maintain the integrity and consistency of the slurry for future use.

After a comprehensive review of all design parameters, a CAD model of the Liq-



uid Jet Polishing (LJP) machine was developed. The resulting model represents the finalized prototype configuration, as illustrated below:-

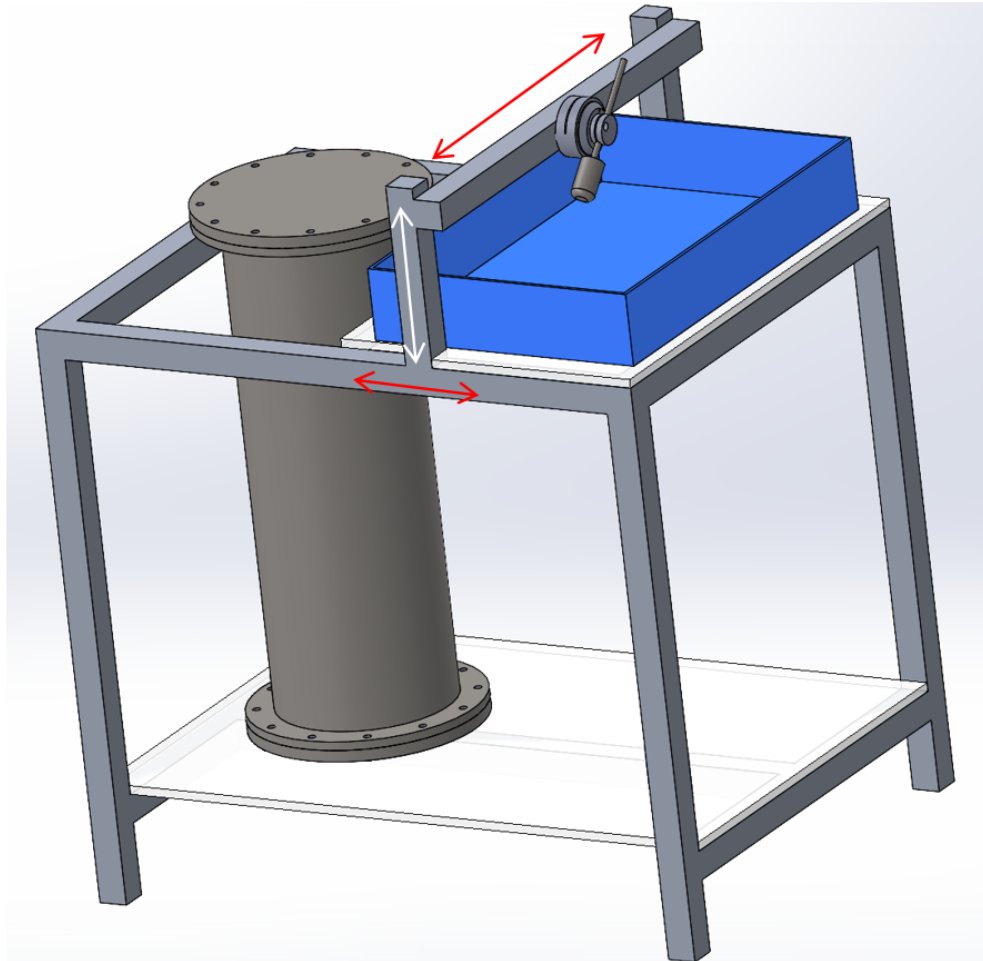


Figure 3.18: CAD model of LJP polishing

### 3.3.10 Integration Setup of Liquid Jet Polishing :-

We have successfully developed a Liquid Jet Polishing (LJP) setup, which has been installed in the Opto-Mechanical Laboratory at RRCAT. The system is designed with a total of six degrees of freedom (DOF). Out of these, four DOF are associated with the nozzle, which is mounted on a combination of a goniometer and a linear excursion stage. The remaining two DOF are provided by a motorized X-Y stage that allows movement in two dimensions.

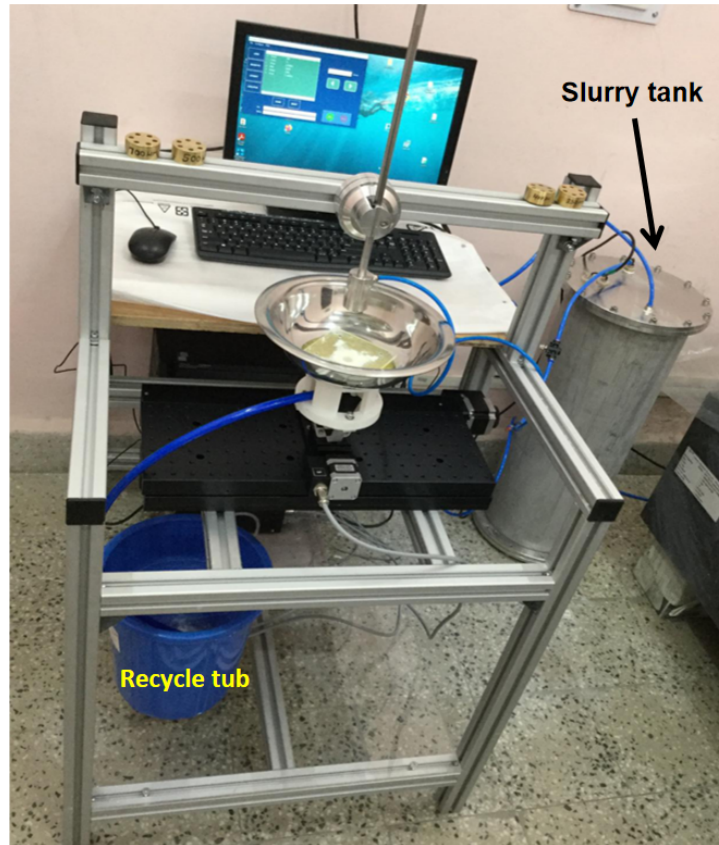


Figure 3.19: Developed FJP setup in RRCAT LAB

As shown in Figure (3.19), the motorized X-Y stage is used to scan the sample surface in the X and Y directions. This stage is controlled through software named Micro Motion HSMC1109, which is installed on a computer connected to the motorized stage.

#### **Working of Prototype liquid jet polishing:-**

In this setup, the polishing slurry a mixture of water and abrasive particles (10:1) is stored in a sealed tank. The tank is equipped with two connections: an inlet and an outlet, both using push-in and push-out fittings.

To operate the system, compressed air at 8 bar pressure is applied through the inlet. This pressure forces the slurry out of the tank through the outlet, which is connected to a nozzle via a 4 mm pipe. The slurry is continuously mixed inside the tank using a stirrer motor. This is necessary because, without mixing, the abrasive particles tend to settle at the bottom due to gravity, which can affect the consistency and effectiveness of the polishing process.

When pressure is applied, the slurry flows through the pipe and exits the nozzle at high speed. The jet then impacts the surface of the optical sample, allowing for precise material removal and polishing.

To control the movement of the sample, a motorized stage is used. This stage can move the sample in two horizontal directions (X and Y axes). The stage is connected to a computer, where speed and distance parameters can be manually set depending on the desired polishing pattern or experimental condition.

After the polishing process, the used slurry is collected in a recycling tub. This tub is connected to the optical table by an 8 mm pipe, allowing the slurry to flow out for reuse.

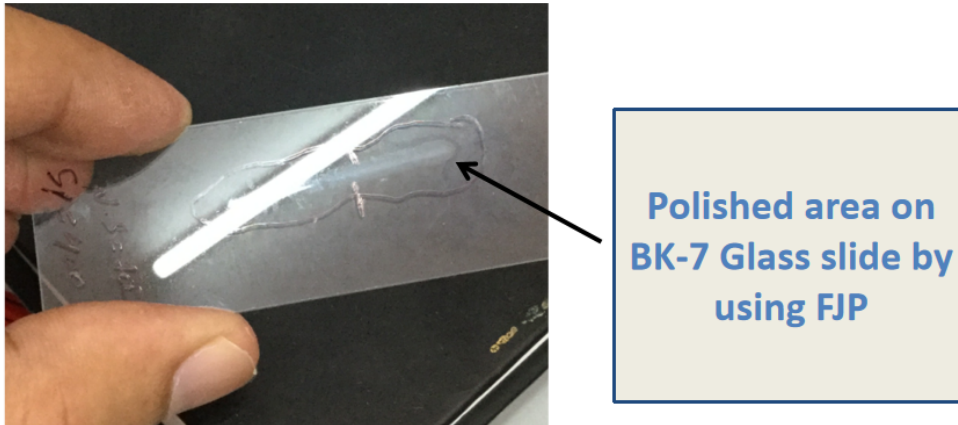


Figure 3.20: Image of polished sample in RRCAT LAB

This entire setup was developed in the laboratory at RRCAT (Raja Ramanna Centre for Advanced Technology). For our experiments, we used BK7 glass plates as the sample material. By adjusting different process parameters, we observed the shape and surface finish resulting from the polishing process, which are shown in the corresponding figures. which will be discussed in the next chapter.

# Chapter 4

## Results and discussion

Liquid Jet Polishing (LJP) technique to remove material from a BK7 glass plate, the polished area takes on a specific shape or pattern. This shape is formed by the jet impacting the surface and depends on the nozzle size, pressure, and polishing time. The result is a smooth, precisely controlled polished spot on the glass.

Experiments were done to assess the efficacy of the LJP system by measuring the material removal for different exposure times for the given set parameters i.e.

- (i) Pressure  $\approx 8$  bar.
- (ii) Nozzle diameter 250 micron, 400 micron, 700micron, 1mm.
- (iii) Stand-off distance (SOD) 5mm.

Efforts were made to assess the dig dimension made by the liquid jet for the give exposure time.

### 4.1 Measurement by using Fizeau interferometer

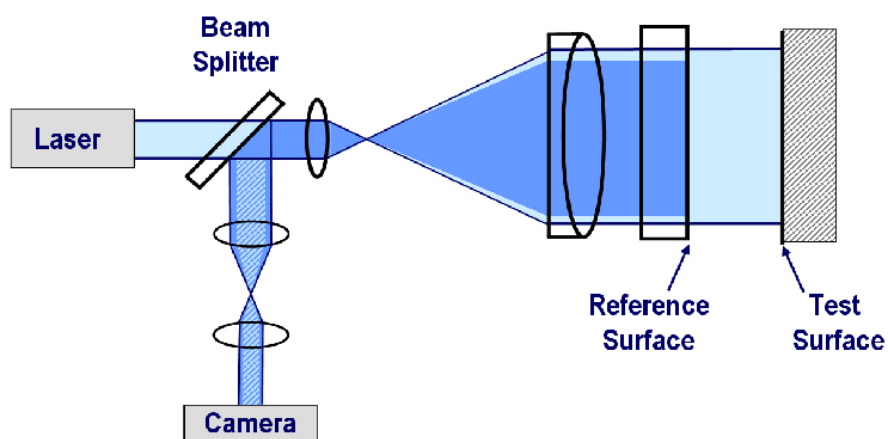


Figure 4.1: Image of Fizeau Interferometer Schematic from ref [11]

To assess the efficacy of the LJP system, initially, two glass sample were processed for 60s and 90s. Fo the whole duration of exposure the jet was fixed at the same location. No relative movement was given between the sample and the jet head. The material removed for the two cases, i.e. 60s and 90s exposure to liquid jet, was imaged with Fizeau Interferometer.

Fizeau interferometer is a non-contact optical measurement technique based on interference of light. A light beam is split into two paths one reflects off a reference surface, and the other reflects off the test surface. When they recombine, the resulting interference pattern (fringes) reveals information about the surface being measured.

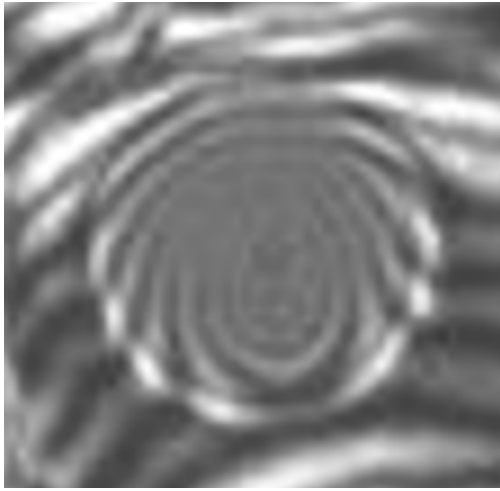


Figure 4.2: Images of fringes acquired with Fizeau Interferometer for 60s

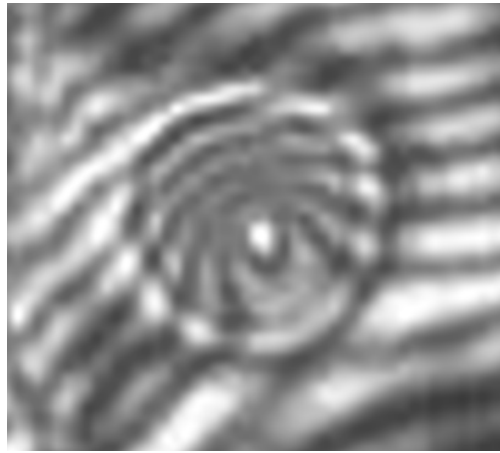


Figure 4.3: Images of fringes acquired with Fizeau Interferometer for 90s

Figure (4.2 and 4.3) shows the photographs (acquire from fizeau interferometer) of the surface map of the BK7 glass plates exposed to 60s and 90s time duration. The surface map of the sample plates were acquired using Zygo interferometer. The observed width of the dig was 3 mm and 4 mm for 60s and 90s exposure time. The dig was found to be deeper for 90s sample, indicating more material removal. In contrast, with a polishing time of 60 seconds, the dig was shallower and the surface appeared cleaner. The images Figure (4.2 and 4.3) show the fringe shift due to surface dig formed by LJP system. The high spatial frequency corresponding to the diameters of the digs ( 3-4mm) is difficult to resolve using a 6 inch Zygo interferometer. Therefore, a transmission mode diffraction phase interferometer was developed to image quantify the material removal of the sample processed under LJP system.

## 4.2 Measurement by using Diffraction Phase Imaging

In transmission mode, data acquired from the DPI (Diffraction Phase Image) technique shows that approximately 700 nm dig were formed at the selected point after 60 seconds of jet impact, as shown in Fig. (d).

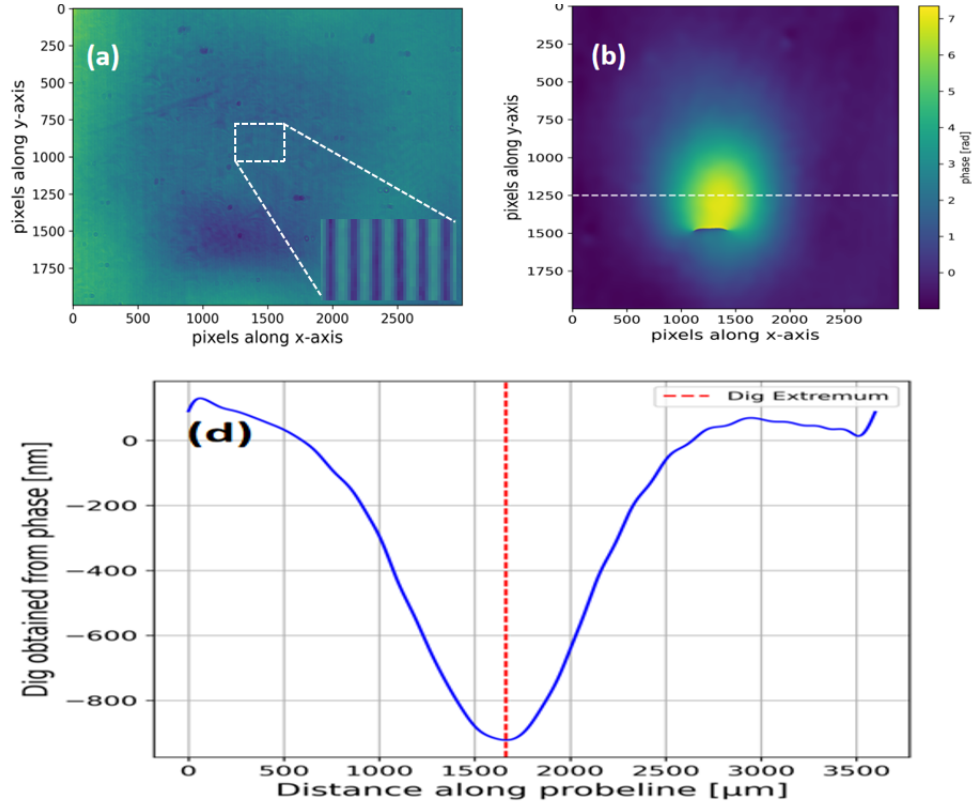


Figure 4.4: image of DPI analysis for 60 sec

Figure (a) shows a representative interferogram of the test sample (60s exposure time) and the corresponding unwrapped phase map after eliminating the background (Fig b). Fig (d) shows the height of the dig developed on the glass slide using LJP system across 1250th row of the phase map (Fig b). Test sample exposed to 60s under LJP shows about a micrometer depth of material removed from the surface of tested glass.

An interferogram of the test surface was first captured, revealing visible interference fringes, as shown in the inset image (a). These fringes indicate surface changes resulting from the liquid jet polishing process. After background removal, an unwrapped phase map was obtained, clearly showing localized phase variations due to material removal. A cross-sectional phase profile was then extracted along the 1250th row of the phase map to analyze the phase change in detail. This profile, shown in radians, highlights the shape and depth of the polished region.

Finally, the phase data was converted into height measurements in nanometers, re-

vealing that the dig created by the Liquid jet polishing process reached a maximum depth of approximately 800 nm at its center. This confirms the capability of liquid jet polishing to produce controlled and localized surface modifications, with DPI providing accurate and detailed analysis of the surface topography.

## 4.2.1 Calibration of DPI

To verify the accuracy of our Diffraction phase imaging system, we carried out a calibration experiment using a standard microscope slide that was  $\approx 1\text{mm}$  thick. A horizontal material removal profile was carefully created on the surface of the slide using the liquid jet polishing system. The material removal profile was made with nozzle diameter of 700 micrometers, and the sample stage was moved at a speed of 400 micrometers per second during the process.

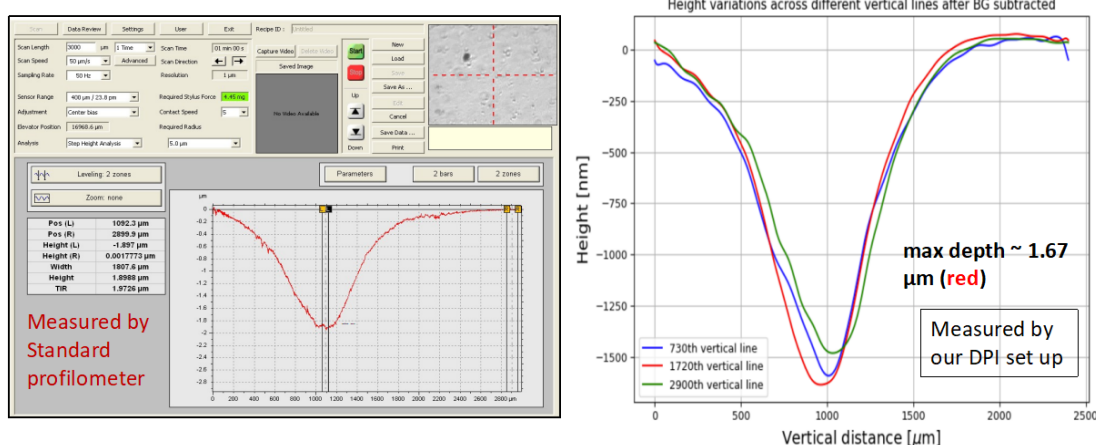


Figure 4.5: Image of data comparison nozzle diameter 700 micron and speed 400 micron/sec

Once the groove like structure is made on the slide, the surface profile is measured using two different methods: Stylus-Based Profilometer and Diffraction Phase Imaging

We used a stylus profilometer made by KLA Tencor (Model: Alpha Standard Stylus Profiler). This device has a sharp tip that moves across the surface and physically touches it to measure surface height changes. To ensure a fair comparison, both measurements were taken at the same location on the sample.

Both the stylus profilometer and our DPI system provided similar results for the material removal profile. This confirms that our DPI system is capable to produce reasonably accurate and reliable surface measurements, matching the performance of a trusted, industry-standard instrument.



#### 4.2.2 Measurement of BK-7 Glass plate polishing by using LJP at various paramter

(a) Nozzle diameter: 1mm, Speed of the sample-stage: 100 micrometer/sec

This data is obtained using Diffraction phase imaging in transmission mode, following polishing process of a BK7 glass plate. The polishing was performed using Liquid Jet Polishing (LJP) with a nozzle diameter of 1 mm and a sample-stage speed of 100  $\mu\text{m/s}$ .

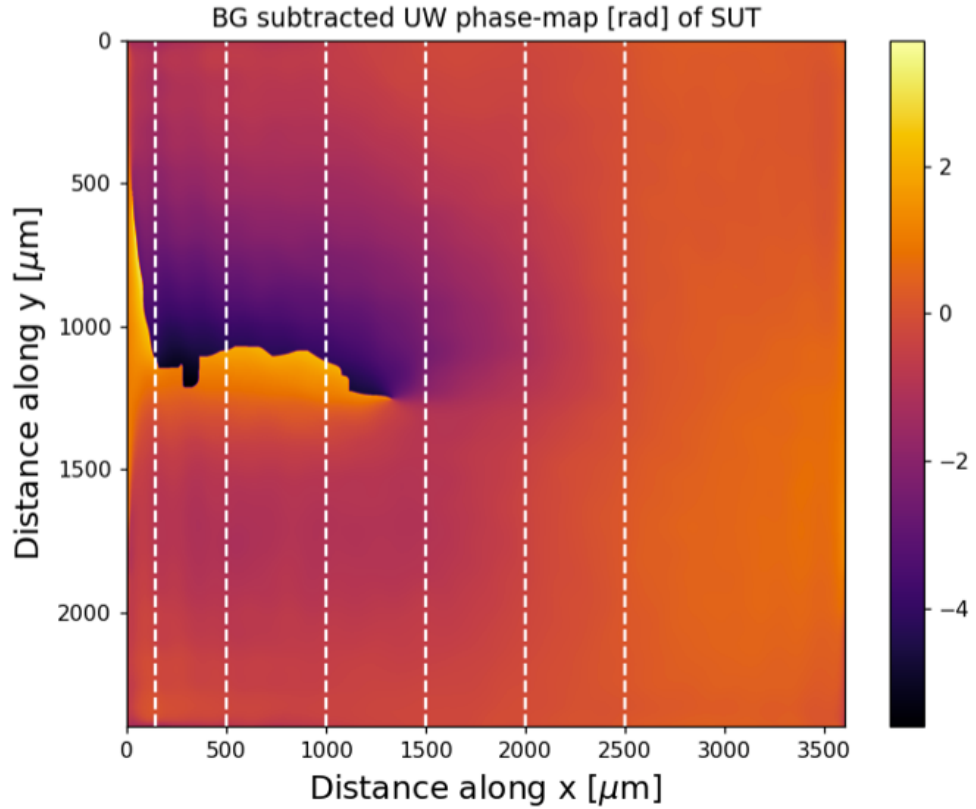


Figure 4.6: 2D phase map for nozzle diameter 1 mm and speed 100 micron/sec

Figure (4.6) shows a 2D phase map where background (BG) phase has been subtracted. This map illustrates the phase variation across the surface of the polished glass sample. The color scale on the right indicates the phase values in radians. Variations in color represent different surface heights, with darker areas indicating valleys (lower height) and brighter areas showing peaks (higher regions). Dashed white vertical lines are marked to show specific x-locations from which height profiles were extracted.

Figure (4.7) presents the height variations (in nanometers) along several vertical lines taken from the phase map. These lines correspond to different positions across the surface (e.g., 145<sup>th</sup>, 500<sup>th</sup>, 1000<sup>th</sup> vertical line, etc.). This graph allows us to analyze how the surface height changes along the y-direction at multiple x-positions.



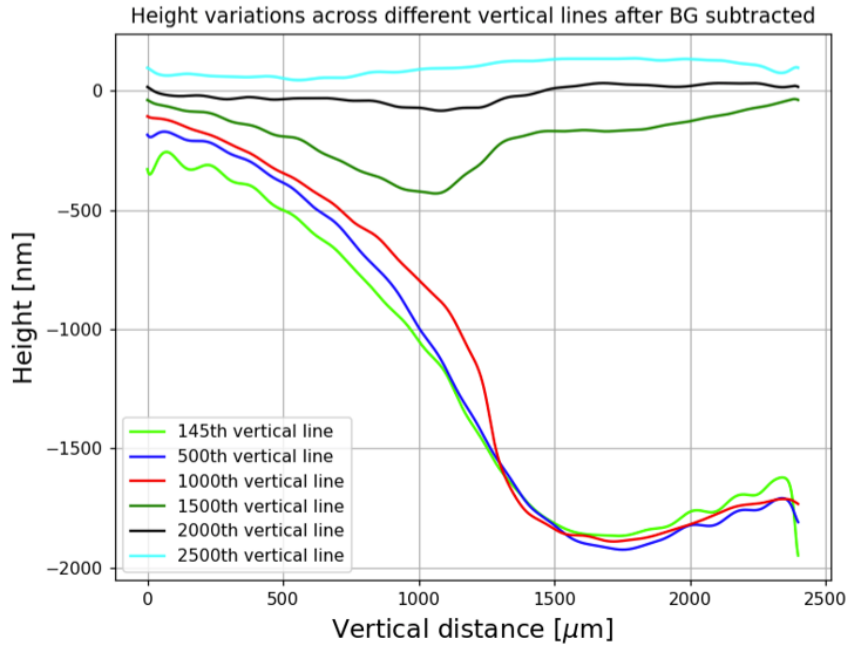


Figure 4.7: Graphical data for nozzle diameter 1 mm and speed 100 micron/sec

From the plot, it is clear that the polishing process has caused significant material removal in some regions (up to nearly 2000 nm in depth), with variation across different locations. This data is not accurate data so we are moving further analysis on different data.

**(b) Nozzle diameter: 1 mm Speed of the sample-stage  $200 \mu\text{m/s}$**

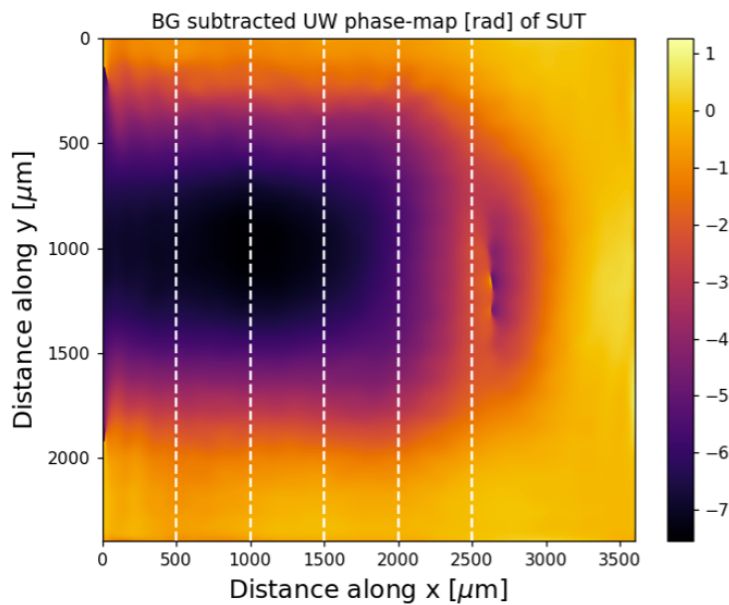


Figure 4.8: 2D phase map for nozzle diameter 1 mm and speed  $200 \mu\text{m/s}$

Diffraction phase imaging in transmission mode after removing material from a BK7 glass plate. The polishing was done using Liquid Jet Polishing (LJP) with a 1 mm nozzle and the sample was moved at a speed of  $200 \mu\text{m/s}$ .

The color scale represents the optical path length difference, with values in radians. The darker regions (towards purple/black) indicate more material removal. Vertical white dashed lines mark specific x-positions where cross-sectional height data has been extracted.

This graph displays height variations (in nanometers) along the y-direction for several selected vertical lines

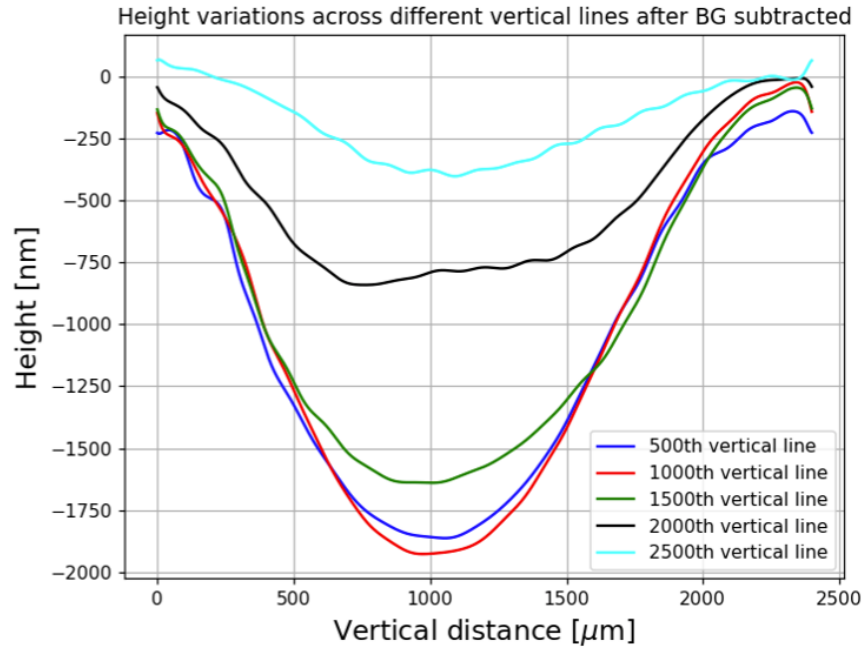


Figure 4.9: Graphical data for nozzle diameter 1 mm and speed  $200 \mu\text{m/s}$

(e.g., 500<sup>th</sup>, 1000<sup>th</sup>, 1500<sup>th</sup>, 2000<sup>th</sup>, 2500<sup>th</sup> lines) which is shown in Figure (4.9). These profiles are derived from the phase map after converting phase to height. The curves reveal a significant concave depression formed due to material removal by the LJP process, with the maximum depth approaching 900 nm. Each curve represents how the depth profile varies across different x-locations on the surface.

**(c) Nozzle diameter: 1 mm, Speed of the sample-stage:  $400 \mu\text{m/s}$**

Figure (4.10) presents the results of a surface analysis experiment involving a 1 mm diameter nozzle and a sample stage moving at a speed of 400 micrometers per second. The figure (4.10) plot shows a two-dimensional phase map of the surface under test (SUT), labeled as “BG subtracted UW phase-map [rad] of SUT”. Here, “BG subtracted” indicates that background signals have been removed, allowing for a clearer representation of the actual surface features.

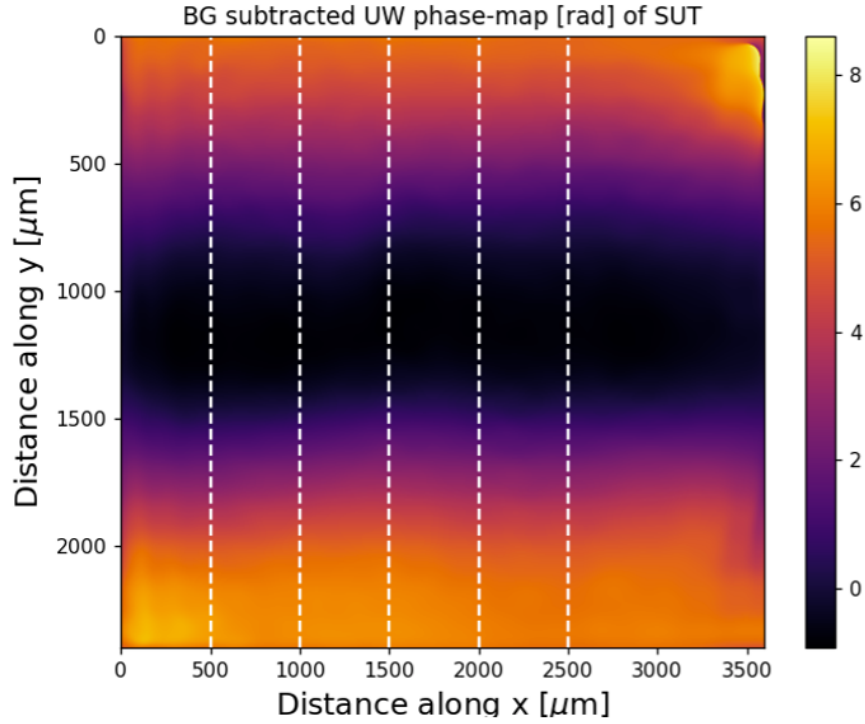


Figure 4.10: 2D phase map for nozzle diameter 1 mm and speed  $400 \mu\text{m}/\text{sec}$

The map uses a color scale to represent phase values in radians, which correlate to height differences across the surface. The x-axis represents the horizontal distance in micrometers, while the y-axis represents the vertical distance. Few white dashed lines mark specific vertical positions used to observe the height variations to quantify the dig-depth done by our LJP system.

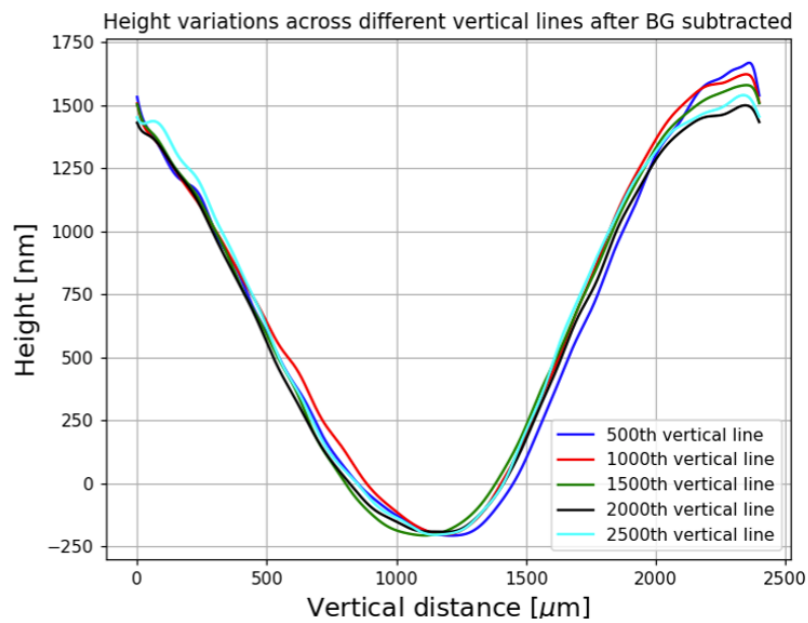


Figure 4.11: Graphical data for nozzle diameter 1 mm and speed  $200 \mu\text{m}/\text{sec}$

The Figure (4.11) displays the height variations along these marked vertical lines. It is titled “Height variations across different vertical lines after BG subtracted”. This graph plots height (in nanometers) against vertical distance (in micrometers), showing how the surface height changes along five selected vertical lines (500<sup>th</sup>, 1000<sup>th</sup>, 1500<sup>th</sup>, 2000<sup>th</sup>, and 2500<sup>th</sup> pixel columns). Each colored line represents a height profile taken from the corresponding vertical position on the phase map. The curves indicate a symmetrical valley like on the surface.

**(d) Nozzle diameter: 700  $\mu\text{m}$ , Speed of the sample-stage: 200  $\mu\text{m}/\text{sec}$**

Figure (4.12) presents surface analysis data from an experiment using a 700  $\mu\text{m}$  diameter nozzle, with the sample stage moving at a slower speed of 200  $\mu\text{m}/\text{sec}$ . In figure (4.12) color-coded phase map titled “BG subtracted UW phase-map [rad] of SUT” where “BG subtracted” indicates that background noise has been removed.

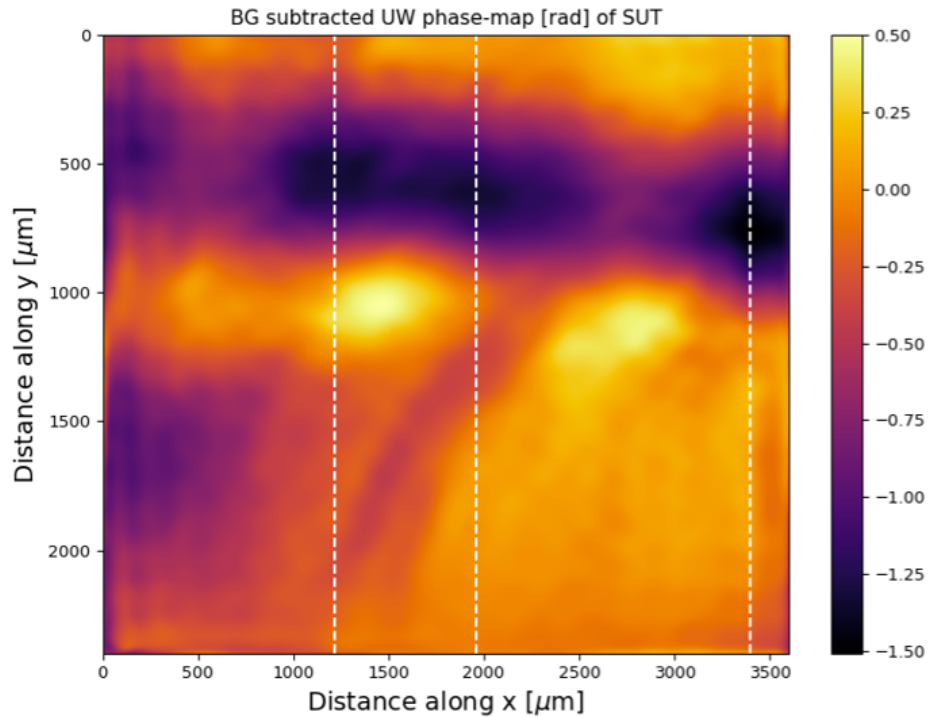


Figure 4.12: 2D phase map [rad] for nozzle diameter 700  $\mu\text{m}$  and speed 200  $\mu\text{m}/\text{sec}$

The phase values are measured in radians and relate to surface height changes across the scanned area. The color scale ranges from -1.5 to 0.5 radians, with dark areas representing depressions and brighter areas indicating raised features.

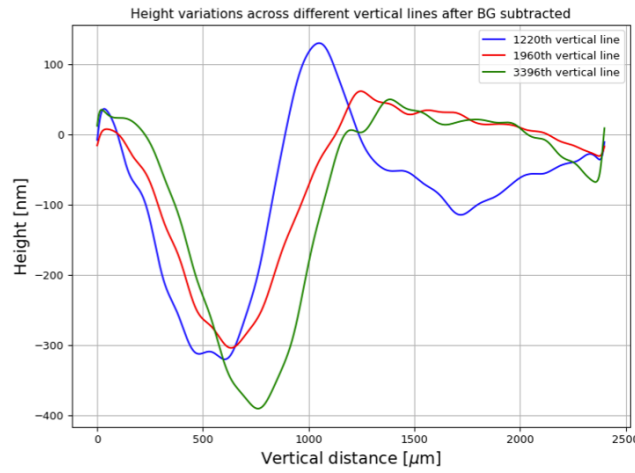


Figure 4.13: Graphical data for nozzle diameter  $700\ \mu\text{m}$  and speed  $200\ \mu\text{m}/\text{sec}$

The height plot profiles corresponding to three of these vertical lines—specifically the  $1220^{\text{th}}$ ,  $1960^{\text{th}}$  columns after converting the phase data into physical height values in nanometers. These curves illustrate how the surface height varies at different locations across the sample shown in Figure (4.13). Unlike the previous image, the height variation here is less symmetrical and shows more irregularities, including a deeper valley and multiple peaks. This suggests that the material or liquid dispensed through the  $700\ \mu\text{m}$  nozzle at a slower stage speed produced a more complex or uneven pattern on the surface.

**(e) Nozzle diameter:  $700\ \mu\text{m}$ , Speed of the sample-stage:  $400\ \mu\text{m}/\text{sec}$**

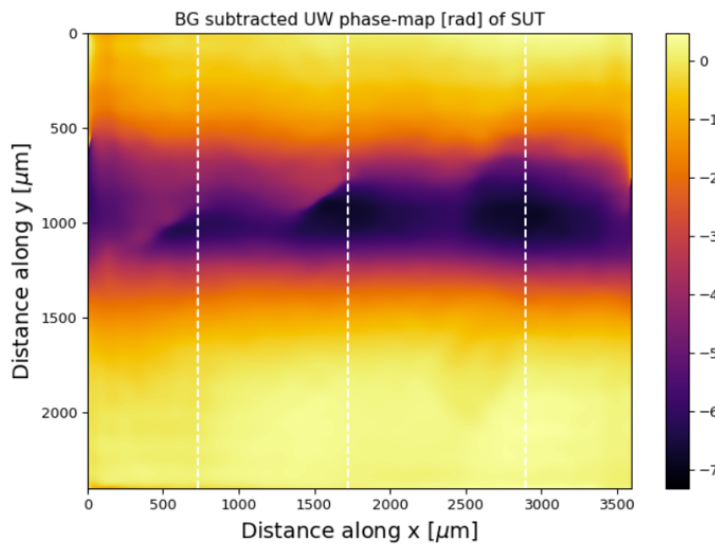


Figure 4.14: 2D phase map for nozzle diameter  $700\ \mu\text{m}$  and speed  $400\ \mu\text{m}/\text{sec}$

In the figure (4.14), phase data shown had background removed to focus only on the effect of the liquid jet on the surface of slide. The color scale represents phase in radians, which relates directly to height or thickness changes on the surface. The dark central region in the plot indicates material removal area, while the yellow regions indicate unaffected areas.

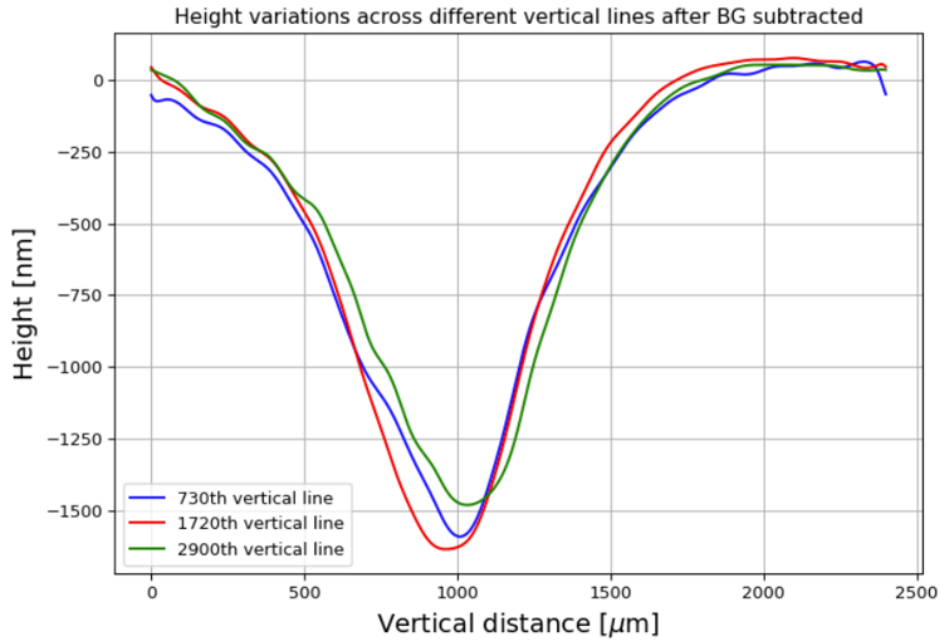


Figure 4.15: Image of Graphical data for nozzle diameter  $700\text{ }\mu\text{m}$  and speed  $400\text{ }\mu\text{m/sec}$

The height of the surface changes vertically (along the y-axis of the phase map) at three of the marked vertical positions: the 730<sup>th</sup>, 1720<sup>th</sup> and 2900<sup>th</sup> vertical lines. All three lines show a smooth and symmetrical dip, indicating a consistent valley shaped formed across the surface. This shape suggests that the material removal from the glass slide is created a clean and uniform trace, possibly due to the balanced combination of nozzle size ( $700\text{ }\mu\text{m}$ ) and faster movement of the sample stage ( $400\text{ }\mu\text{m/sec}$ ), resulting in an even and well-distributed material-removal from the surface.

# Chapter 5

## Conclusions and Future scope

In this thesis work a low coherent interferometry based Diffraction phase imaging system was developed for imaging the samples processed by liquid jet polishing system.

Diffraction Phase Imaging (DPI) is an optical imaging technique that utilizes the principles of diffraction and interference of light to create high-resolution images of transparent samples [4]. In the developed DPI system, the incident light was splitted in multiple beams by means of a grating beam splitter that diffracts beam in multiple diffraction orders. A mask blocks all the beams except zero and first order beams. This mask also involves a pin hole that removes the higher spatial frequency light generated due to the sample. The filtered zero order beam act as the reference wave and interfere with the +1 order diffracted light on the charge coupled device (CCD) sensor. As both the sample and reference light are originated from the same sample and both travel adjacent to each other, the system behaves like common path Mach-Zehnder interferometer. The phase shift retrieve by processing of these interference patterns. DPI is capable to reconstruction of phase maps with high precision down to nanometer scale. Therefore a transmission mode DPI system was developed to characterize the optical glass substrate samples processed with LJP system.

A prototype Liquid Jet Polishing (LJP) system was also developed that removes the material from the glass plate using a high pressure jet of abrasive slurry. It is a non-contact, deterministic, and flexible material removal technique. This method is particularly useful for delicate materials like optical glasses, where traditional mechanical methods may introduce sub surface damage as well as uneven removal and also this method is know as point by point polishing method.

The developed Liquid jet polishing setup consists of a controlled abrasive slurry jet that is directed through a nozzle onto the surface of a sample mounted on a motorized translation stage. The experimental setup allowed control over several important process parameters, including nozzle diameter, jet pressure, stand-off distance (distance between the nozzle and the surface), and the speed of the sample stage. These parameters were varied and monitored in initial trials to assess the removal characteristics of

the system and its overall effectiveness in material removal and surface shaping.

Results of initial experiments to explore the efficacy of the developed system show that, 1 mm nozzle diameter and 5 mm stand off distance is able to remove the material to form digs of diameter of 3 mm and 4 mm size in 60 sec and 90 sec respectively. A developed transmission mode diffraction phase imaging system is also used to assess the material removal using the prototype LJP system.

Based on the experimental observations and surface characterization results, it was found that the LJP system is capable of effective removal of material from BK-7 glass plate in a controlled manner. One of the significant outcomes observed during the trials was the formation of a smooth and symmetrical “dig” on the substrate surface after polishing. The depth of the dig was calculated to be approximately  $1.67\ \mu\text{m}$ , indicating successful and measurable material removal. The phase maps and height profiles generated through background-subtracted interferometric measurements confirmed the consistency and symmetry of the polished regions, especially when optimized parameters were used (e.g.,  $700\ \mu\text{m}$  nozzle with  $400\ \mu\text{m}/\text{sec}$  stage speed).

The comparison of different nozzle diameters and stage speeds also provided insight into how each parameter affects the material removal rate and surface quality. For example, larger nozzles resulted in deeper material removal, while faster speeds and smaller nozzles produced shallower and more uniform results.

Thus, from the initial testing and analysis, it can be concluded that the prototype LJP system demonstrates promising potential for precision polishing, especially for optical materials such as glass slide. The system is capable of achieving localized, damage-free polishing with controlled depth and shape, which is a critical requirement in optical component fabrication.

## **Future Scope**

While the preliminary experiments have proven the basic functionality and effectiveness of the LJP system, several opportunities exist to further improve and expand its capabilities. The future scope of this work includes the following areas of development:

### **(A) Process Optimization for Ultra-Polishing**

The current LJP setup successfully demonstrates material removal, but further work is required to optimize the process for high-precision polishing. This includes fine-tuning process parameters such as slurry composition, jet pressure, nozzle stand-off distance, nozzle geometry, dwell time, and translation path strategies. The aim is to reduce surface roughness further and achieve a highly polished surface suitable for high-performance optical components.



## **(B) Integration of Liquid jet polishing with diffraction phase imaging System**

One of the key future improvements will be the integration of a Diffraction phase imaging system into the LJP setup. DPI systems provide real-time surface data, which can be used to monitor the polishing process as it occurs. By implementing online surface measurement, it becomes possible to dynamically adjust polishing parameters in response to the observed surface condition.

# Bibliography

- [1] KG Anbarasu, L Vijayaraghavan, and N Arunachalam. Effect of multi stage abrasive slurry jet polishing on surface generation in glass. *Journal of Materials Processing Technology*, 267:384–392, 2019.
- [2] Anthony Beaucamp, Yoshiharu Namba, and Richard Freeman. Dynamic multiphase modeling and optimization of fluid jet polishing process. *CIRP annals*, 61(1):315–318, 2012.
- [3] Zhong-Chen Cao, Ming Wang, Shengqin Yan, Chenyao Zhao, and Haitao Liu. Surface integrity and material removal mechanism in fluid jet polishing of optical glass. *Journal of Materials Processing Technology*, 311:117798, 2023.
- [4] Sanjit K Debnath, Yogesh Verma, and Pradeep K Gupta. White light diffraction phase microscopy as profilometry tool. *Optical Engineering*, 53(9):092008–092008, 2014.
- [5] VV Demjanov. What and how does a michelson interferometer measure. *arXiv preprint arXiv:1003.2899*, 2010.
- [6] Oliver W Föhnle, Hedser Van Brug, and Hans J Frankena. Fluid jet polishing of optical surfaces. *Applied optics*, 37(28):6771–6773, 1998.
- [7] Hui Fang, Peiji Guo, and Jingchi Yu. Surface roughness and material removal in fluid jet polishing. *Applied optics*, 45(17):4012–4019, 2006.
- [8] Zongfu Guo, Tan Jin, Li Ping, Ange Lu, and Meina Qu. Analysis on a deformed removal profile in fjp under high removal rates to achieve deterministic form figuring. *Precision Engineering*, 51:160–168, 2018.
- [9] Parameswaran Hariharan. *Basics of interferometry*. Elsevier, 2010.
- [10] <http://hyperphysics.phy.astr.gsu.edu/hbase/phyopt/fabry.html>1.
- [11] <https://4dtechnology.com/products/fizeau-interferometer/>.
- [12] <https://bigthink.com/starts-with-a-bang/failed-experiment-einstein-revolution/>.

- [13] <https://bme240.eng.uci.edu/students/07s/jjiang/basic>
- [14] <https://www.newport.com/n/diffraction-grating-physics>.
- [15] [https://www.researchgate.net/figure/Michelson-interferometer-1\\_fig3\\_330423929](https://www.researchgate.net/figure/Michelson-interferometer-1_fig3_330423929).
- [16] [https://www.researchgate.net/figure/Schematic-diagram-of-the-maskless-fluid-jet-polishing-MFJP-of-structured-surface\\_fig1\\_354920717](https://www.researchgate.net/figure/Schematic-diagram-of-the-maskless-fluid-jet-polishing-MFJP-of-structured-surface_fig1_354920717).
- [17] [https://www.shutterstock.com/search/laser-interferometry-image\\_type=illustration](https://www.shutterstock.com/search/laser-interferometry-image_type=illustration).
- [18] David Huang, Eric A Swanson, Charles P Lin, Joel S Schuman, William G Stinson, Warren Chang, Michael R Hee, Thomas Flotte, Kenton Gregory, Carmen A Puliafito, et al. Optical coherence tomography. *science*, 254(5035):1178–1181, 1991.
- [19] Y. Verma-S. Raja S. S. Chakraborty, P. Sharma. White light diffraction phase microscopy as profilometry tool. *Poster presentation in National Laser Symposium-32, RRCAT, Indore*, 2024.
- [20] Bahaa EA Saleh and Malvin Carl Teich. *Fundamentals of photonics*. Wiley New York, 2008.
- [21] Mitsuo Takeda, Hideki Ina, and Seiji Kobayashi. Fourier-transform method of fringe-pattern analysis for computer-based topography and interferometry. *Journal of the optical society of America*, 72(1):156–160, 1982.
- [22] Zebin Xia, Fengzhou Fang, Eamonn Ahearne, and Moran Tao. Advances in polishing of optical freeform surfaces: a review. *Journal of Materials Processing Technology*, 286:116828, 2020.
- [23] Zili Zhang, Chi Fai Cheung, Chunjin Wang, and Jiang Guo. Modelling of surface morphology and roughness in fluid jet polishing. *International Journal of Mechanical Sciences*, 242:107976, 2023.